AD_____

Award Number: DAMD17-97-1-7341

TITLE: The Use of NF1 and NF2 Mutant Mouse Strains in the Investigation of Gene Function and Disease Development

PRINCIPAL INVESTIGATOR: Tyler Jacks, Ph.D.

CONTRACTING ORGANIZATION: Massachusetts Institute of Technology
Cambridge, Massachusetts 02139

REPORT DATE: October 2000

TYPE OF REPORT: Final

PREPARED FOR: U.S. Army Medical Research and Materiel Command
Fort Detrick, Maryland 21702-5012

REPORT DOCUMENTATION PAGE

Form Approved
OMB No. 074-0188

1. AGENCY USE ONLY (Leave blank)	2. REPORT DATE	3. REPORT TYPE AND DATES COVERED
	October 2000	Final (30 Sep 97 - 29 Sep 00)

4. TITLE AND SUBTITLE
The Use of NF1 and NF2 Mutant Mouse Strains in the Investigation of Gene Function and Disease Development

5. FUNDING NUMBERS
DAMD17-97-1-7341

6. AUTHOR(S)
Tyler Jacks, Ph.D.

7. PERFORMING ORGANIZATION NAME(S) AND ADDRESS(ES)
Massachusetts Institute of Technology
Cambridge, Massachusetts 02139

E-MAIL:
tjacks@mit.edu

8. PERFORMING ORGANIZATION REPORT NUMBER

9. SPONSORING / MONITORING AGENCY NAME(S) AND ADDRESS(ES)
U.S. Army Medical Research and Materiel Command
Fort Detrick, Maryland 21702-5012

10. SPONSORING / MONITORING AGENCY REPORT NUMBER

11. SUPPLEMENTARY NOTES

12a. DISTRIBUTION / AVAILABILITY STATEMENT
Approved for public release; Distribution unlimited

12b. DISTRIBUTION CODE

13. ABSTRACT ***(Maximum 200 Words)***

Mouse strains carrying germline mutations in the NF1 and NF2 tumor suppressor genes have been used as mouse models for human neurofibromatosis types 1 and 2. Progress over the past 3 years has included the generation of three mouse models of NF1. These models include a chimeric model, which develops benign neurofibromas; a combined germline NF1/p53 mutant model that develops MPNSTs; and a combined NF1/p53 mutant model that develops astrocytomas. Through biochemical analysis of the Nf1 gene product we have identified a mechanism by which neurofibromin is regulated, the sequences responsible for this regulation, and the role of neurofibromin in attenuating the Ras/MAP kinase pathway in MEFs. Genetic modifier screens using the NF1/p53 mice on different inbred strain combinations have been performed. All F1 strain combinations show significant differences in tumor latency and/or tumor spectra when compared to the B6 parental strain. In addition, different backcross strains are being generated to identify modifier genes. Progress is reported toward the development of an in vitro kinase assay for the isolation of a kinase responsible for phosphorylating the Nf2 gene product, merlin. Finally, Nf2 conditional expression systems have been developed to assess Nf2 function in growth control, tumor suppression, and cell survival.

14. SUBJECT TERMS
Neurofibromatosis

15. NUMBER OF PAGES
33

16. PRICE CODE

17. SECURITY CLASSIFICATION OF REPORT	18. SECURITY CLASSIFICATION OF THIS PAGE	19. SECURITY CLASSIFICATION OF ABSTRACT	20. LIMITATION OF ABSTRACT
Unclassified	Unclassified	Unclassified	Unlimited

Table of Contents

Introduction

Neurofibromatosis type I and II (NF1 and NF2) are human genetic diseases affecting the nervous system. The approach of our laboratory to the study of the NF1 and NF2 genes and their associated diseases has been to construct mouse strains with targeted mutations in the murine homologues of NF1 and NF2. Mouse models of both NF1 and NF2 have been generated and used for the characterization of the diseases. Cells derived from mutant animals have been utilized to assess the biochemical role of Nf1 and Nf2 in growth control, tumor suppression, and cell survival.

Body

This final report has been divided into sections corresponding to the Technical Objectives/specific Aims of the original grant, which was initiated on 30 September 1997.

1. Characterization and manipulation of the murine model of NF1. Murine models for neurofibroma and MPNST development have been successfully generated and characterized as described in the 1998-1999 progress report. These data have also been published (1) and therefore will not be discussed further here.

A genetic modifier screen using the Nf1/p53 strain was conducted. The resulting astryocytoma/glioblastoma model was recently published (2) and will not be discussed further here.

Although the Nf1-/- chimera model provides an important model for addressing the differences in phenotype between NF1/*Nf1* mutant humans and mice as well as an avenue for tumor analysis, it is a difficult model with which to work. The main difficulty is the percentage of chimeric embryos that survive to term, even following injection of 1-2 Nf1-/- cells. Therefore, we do not plan to pursue this model further at this time. Instead, we have contacted Luis Parada (UT, Dallas), who has made a conditional loss-of-function allele of *Nf1*. In 2001, we plan to initiate experiments to develop mouse models of neurofibroma formation using the Parada, conditional *Nf1* mouse.

Finally, over the past several months, we have begun a differential cDNA-cloning project to isolate genes differentially expressed in Nf1-/- cells. A subtractive hybridization was performed to isolate genes that are upregulated in *Nf1-/-* mouse embryonic fibroblasts (MEFs) that survive in the absence of growth factors. The "driver" population was composed of a mixture of cDNA derived from wild-type MEFs grown in 0.1% serum (these cells are alive but quiescent) and cDNA derived from serum-starved wild-type MEFs (at a time when a significant portion of the cells were undergoing apoptosis) and a "tester" population of cDNA derived from Nf1 -/- cells in serum-starved conditions (which survive inappropriately). Numerous cDNAs were found to be significantly upregulated in the Nf1 -/- cells, but identification of these cDNAs has proven difficult. For this reason, we have initiated microarray analysis to compare these cDNA populations. The use of Affymetrix Genechip arrays will allow us to readily identify cDNAs that are both upregulated and downregulated in the Nf1 -/- cells, because all of the oligos on the array represent known genes and ESTs.

2. Structure/function analysis of neurofibromin. As described in the 1999 progress report, we have been examining the mechanisms that normally regulate neurofibromin protein levels as well as the effects of this regulation on the Ras pathway. We have found that neurofibromin is dynamically regulated by the proteasome in a protein kinase C (PKC) dependent manner. This regulation correlated precisely with the proper regulation and attenuation of the Ras/MAP kinase pathway in mouse embryonic fibroblasts (MEFs) under specific growth conditions (see 1999 report). In the 1999 report, we speculated that a specific PKC phosphorylation event might be involved in triggering neurofibromin degradation. However, by examining neurofibromin deletion mutants an *in vitro* degradation assay, we found that a ten amino acid region, N-terminal to the GAP-related domain, is responsible for this degradation. Thus, we have identified the mechanism by which neurofibromin is regulated, the sequences responsible for this regulation and the role neurofibromin plays in attenuating the Ras/MAP kinase pathway in MEFs. A manuscript describing this work will be submitted shortly.

3. Screen for genes modifying *NF1* or *NF2* in mice. In the previous year, the generation of *Nf1;p53* cis heterozygous mice (NPcis) inbred into both B6 and BALB/c (backcross generation 10 or greater) has been completed. In addition, we have completed the generation of NPcis mice on the 129/Sv background and are in the process of analyzing the tumor phenotype. We have generated *Nf2;p53* cis heterozygous mice on the B6 background and well as the *Nf2;p53;Nf1* triple cis heterozygous mice on the B6 background for comparison to NPcis mice on B6. The generation of *Nf1;Nf2* cis heterozygous mice on the B6 background is currently in progress. The comparison of the 3 double heterozygous strains and the 1 triple heterozygous strains should give us insight into the genetic relationship between these 3 genes in suppressing tumor development.

In the past year, we have completed survival curves for NPcis mice on two inbred strains (B6 and BALB/c) and on 6 F1 strains (AXB6, CBAXB6, C3HXB6, DBA/2XB6, SJLXB6, and CASTXB6). In addition, the tumor spectrum analysis has been completed for all but the DBA/2XB6 strain. All F1 strain combinations show significant differences in tumor latency and/or tumor spectra when compared to the B6 parental strain. The most striking effects seen are 1) a large increase in histiocytic sarcoma in the CASTXB6 strain, 2) a reduction in soft-tissue sarcomas in the AXB6 strain and a commensurate increase in brain tumors, 3) a reduction of lymphoma in the SJLXB6 strain, and 4) the occurrence of leukemia in the CASTXB6 strain, which was never seen in the B6 strain.

To identify the modifier genes acting in these strains, we have focused on aging the NPcis mice on different backcrossed strains in order to map dominantly-acting modifiers. NPcis mice on a (CASTXB6)XB6 background are being used to identify

modifier genes affecting histiocytic sarcoma and leukemia. NPcis mice on a (AXB6)XB6 background are being used to identify modifier genes affecting soft tissue sarcomas. Because thymic lymphoma is seen in roughly 12% of NPcis mice in B6,we have switched to the p53 homozygous null mouse to look for modifier genes affecting lymphoma. Seventy-one percent of p53 null mice on a mixed background develop lymphoma. p53 null mice in a (SJLXB6)XB6 backcross, by crossing p53 mutant mice on SJLXB6 to p53 mutant mice on B6 are currently being generated. All of these backcross studies are ongoing. Data from the backcross studies will give us an indication of how many genes are involved in each of these strain effects, and will be used to map the modifier gene(s) if a small number of strongly-acting genes are involved.

A mouse model for glioblastoma. The NPcis mice inbred onto B6 provide a genetically well-defined system to study human cancer models. In the past year, we have characterized the formation of astrocytomas and glioblastomas in NPcis mice (2). This is one of the first spontaneous astrocytoma models in mice to be generated by mutation of tumor suppressor genes, rather than by transgenic overexpression of oncogenes. We are currently collaborating with researchers at Massachussetts General Hospital to inject cell lines from these tumors intracranially into nude mice to develop a model for the diffuse infiltration seen in human astrocytoma. The diffuse infiltration of astrocytoma cells in human brains makes this cancer essentially incurable, and we hope to better understand the biology of these cells using the mouse model.

To further develop our mouse model of astrocytoma, we have crossed the NPcis mice to other mouse mutants involved in either glioblastoma or neurofibromatosis type 1. *PTEN* is a tumor suppressor mutated in the highest grade of astrocytoma in humans. In the past year we have begun crosses to generate NPcis;*Pten*-/+ mice to examine whether astrocytomas are accelerated to higher grades in these mice. *MSH2* is a member of a family of mismatch repair genes that have been implicated in neurofibromatosis type 1. We have initiated crosses to generate NPcis;*MSH2*-/- mice to examine whether increasing mutation rates in these mice change the tumor phenotype.

This past year we have identified several interesting modifying effects in inbred strains of mice and have begun generating backcross progeny in order to map these effects. We have also developed a mouse model of an incurable human cancer, astrocytoma, and are continuing studies to address the behavior of these tumor cells *in vivo* and *in vitro*.

4. Characterizing *NF2* deficiency in adult chimeras and MEFs. As we have described previously, we have observed an induction of phosphorylation of the Nf2 gene product, merlin, following activation of the Rac-1 signaling pathway (3). In addition, Nf2-/- MEFs have been shown to have increased motility when compared to wild-type

MEFs. This observed increase in motility is consistent with an upregulation of Rac-1 signaling in the cells. Over the last several years, we have examined the interaction of Rac-1 and merlin. In collaboration with a former postdoctoral fellow, Andrea McClatchey (MGH) we have found increased Rac-1 signaling in Nf2-/- cells. We have left further characterization of the Rac-1/merlin signal transduction pathway to Dr. McClatchey and have ourselves focused on the isolation of the merlin kinase, which will be discussed below.

5. Continued investigation of merlin function.

Isolation of the Merlin Kinase. Based on observations described in previous annual reports, it would appear that phosphorylation of merlin may be critical to its regulation. To facilitate the understanding of merlin regulation, we have set out to isolate the Rac-dependent kinase that phosphorylates merlin on Serine 518. Two different approaches have been taken to address this question in parallel. The first is an unbiased approach of biochemical purification of a kinase activity. The second approach is testing various known candidates, either directly activated by Rac/cdc42 or in the downstream signaling pathways, for the ability to phosphorylate merlin.

For both approaches, it was necessary to establish an in-vitro kinase assay to follow merlin phosphorylation. Such an assay requires abundant amounts of substrate protein. As merlin is poorly expressed in bacterial cells, due to insolubility and degradation of the full-length protein, we created a pseudo-substrate. This substrate is composed of a fragment of merlin, flanking the site of phosphorylation, fused to GST. The substrate is easily expressed and purified from bacterial cells and was in 3 different forms: wild-type (Ser518), 518A (Ser518 to Ala) and 518T (Ser518 to Thr). An in-vitro kinase assay has been set up to follow the kinase activity, with the wild-type substrate. To test the validity of this approach all three substrates were tested in a kinase assay with extracts from NIH3T3 cells that were serum treated as described (3).

We have observed that the S518 form of the substrate is phosphorylated. This phosphorylation is specific as the negative control, 518A, is not phosphorylated under these conditions. The fact that 518T is phosphorylated as well serves as an additional indication of specificity. Once specificity had been established, we fine-tuned the assay conditions including levels of substrate and extract, reaction buffer composition, etc. Furthermore, we then applied these conditions to a reaction in which the substrate was substituted with the full-length wild-type or 518A merlin, immunoprecipitated from NIH3T3 cells, and demonstrated the specificity of the in-vitro kinase reaction. In

addition, we showed that the kinase activity towards the pseudo-substrate behaves similarly to the activity of the kinase towards merlin.

Several standard approaches have been assessed for the purification of the merlin kinase. The following steps have been utilized, Ion-exchange chromatography, hydrophobic interaction chromatography, affinity chromatography, and gel-filtration. Various columns and media have been assessed for each purification step in order to work out optimal purification conditions. In addition we have investigated sources of crude protein extracts and determined that the most abundant sources for the kinase activity are tumors generated from NIH3T3 cell transformed with an activated allele of Rac and FO99 fibrosarcoma cell line.

Many serine/threonine kinases are known to be directly or indirectly activated by Rac and/or cdc42. In an initial screen, activated alleles of PAK1, Mkk4, LIM-kinase and PRK2 were co-transfected into NIH3T3 cells with a merlin expression construct. Analysis of merlin hyper-phosphorylation by Western blot demonstrated that these kinases do not mediate the Rac/cdc42-induced phosphorylation of merlin. Other effectors are currently being tested, employing the *in-vitro* kinase assay.

Using kinase inhibitors, we studied the inhibition of the merlin kinase. Several types of inhibitors have been employed including staurosporine. Only Staurosporine inhibited the activity. Although this inhibitor is broad ranged, the fact that the other inhibitors partially overlap in their action, allows eliminating some kinase groups. By this process of elimination the PKA, PKG, MLCK, and CaMKII groups are excluded from containing the merlin kinase.

Conditional Alleles of NF2. We have previously attempted to overexpress *Nf2* in NIH3T3 cells and *Nf2-/-* tumor-derived cell lines without success, presumably because unregulated expression of the protein is toxic or leads to growth arrest. Therefore, in order to study the effects of forced expression of merlin, it was necessary to develop a conditional expression system. For our Nf2 re-introduction studies, we have chosen to use the ecdysone-inducible expression system. Developed for mammalian cells in the laboratory of Ronald Evans, this system allows for dose-dependent, regulated expression of the introduced construct (4). We have inserted full-length wild-type Nf2 cDNAs of the two major isoforms (I and II), versions of these carrying N-terminal epitope tags (HA or FLAG), epitope tagged fragments representing N- and C- terminal halves of the protein, and phosphomutants of serine 518. LLC PK1 epithelial cell lines have been established that can inducibly express different merlin constructs. These lines will be used to assess Nf1 function in growth control, tumor suppression, and cell survival.

We have been interested in examining the growth regulatory pathways in which merlin operates and the consequences of *Nf2* mutation in tumorigenesis. To examine merlin's function in these pathways we have begun by using Nf2-deficient fibrosarcoma and osteosarcoma cell lines derived from tumors in Nf2 +/- mice that have undergone an LOH event at the Nf2 locus. Another source of Nf2 deficient cell lines that we are planning to utilize is MEFs. Previous work from our laboratory and the laboratory of Andrea McClatchey (MGH) has allowed for the generation of Nf2-/- MEFs from Nf2-/- chimeric embryos. Generation of these MEFs requires selection of the harvested cells to ensure a pure population of Nf2-/- cells, and the process has proven to be difficult and often yield few cells for experimentation. Therefore, the MEFs we are planning to use for our studies will be derived from $Nf2^{flox2/flox2}$ and $Nf2^{+/flox2}$ mice (5). We have obtained these conditional mice from Marco Giovannini (INSERM, CEPH) and will be preparing MEFs from these lines in the near future.

6. Therapeutic evaluation of farnesyltransferase inhibitors. Our lab has been interested in the use of mouse disease models to evaluate potential drug therapies . The farnesyltransferase inhibitors, directed against the Ras signaling pathway, are logical candidates for the treatment of tumors with mutations in *NF1*.

As we have discussed in past reports, we have had an ongoing discussion with Merck Pharmaceuticals to supply us with the farnesyltranferase inhibitor L-744,832, which has been used to treat RAS dependent tumors in the past (6,7). Because of the uncertainty concerning the amount of the compound needed to complete such studies, there has been great consideration concerning the mouse models we will test. Ultimately, we have chosen the *Nf1/p53* cis model for astrocytoma and glioblastoma and have been generating B6 congenic mice in order to carefully control our experiments. Mice to be tested have been generated and drug treatment is expected to begin in December 2000.

Key Research accomplishments:

- Mapping of the domains of merlin responsible for subcellular localization (3).
- Generation and characterization of a chimeric model of NF1 which develops benign neurofibromas (1).
- Generation and characterization of a combined germline NF1/p53 mutant model that develops MPNSTs (1).
- Generation and characterization of a combined NF1/p53 mutant model that develops astrocytomas and glioblastomas (2).
- Establishment of assays for the purification of merlin kinase. (manuscript in preparation).
- Demonstration that neurofibromin is regulated by proteolysis in a proteasome dependent manner.. (manuscript in preparation).

Reportable Outcomes:

Manuscripts:

K. Reilly, D.A. Loisel, R.T. Bronson, M.E. McLaughlin, & T. Jacks, *Nature Genetics* **26**, 109-113 (2000).

K. Cichowski, T. S. Shih, E. Schmitt, S. Santiago, K. Reilly, M. McLaughlin, R.T. Bronson, & T. Jacks, *Science* **286**, 2172-2176 (1999).

K.M. R.J. Shaw, A.I. McClatchley, & T. Jacks, *Cell Growth and Differentiation* **9**, 287-296 (1998)

Personnel supported by this grant:

Karen Cichowski, Ph.D.	Postdoctoral fellow
Karlyne Reilly, Ph.D.	Postdoctoral fellow
Reuben Shaw, Ph.D.	Graduate Research Assistant
Shane Shih, Ph.D.	Graduate Research Assistant
Sabrina Santiago	Research Technician

Degrees Received:

Reuben Shaw	Ph.D.
Shane Shih	Ph.D.

Conclusion

In the past three years we have made great progress towards the goals outlined in our grant proposal. We are quite pleased with the success we have had with the Nf1 mouse models. Examination of the Nf1-/-:Nf1+/+ chimeras has indicated an obligate role of Nf1-/- loss in neurofibromin formation. In addition, we have demonstrated a cooperation between Nf1 and p53 in the formation of MPNSts. In order to provide a framework for understanding the consequences of Nf1 mutation in disease we have performed biochemical analysis. We have found that neurofibromin regulation correlates precisely with the regulation of the Ras/MAP kinase pathway in MEFs. We have recently identified the sequences and mechanism by which this regulation occurs. By combining biochemical analysis and the use of mouse models we have come far in elucidating the function of Nf1. Continued study utilizing these two approaches will be crucial to further characterize the tumorigenic mechanisms involved in tumor formation and in the evaluation of potential therapies, such as compounds designed to inhibit Ras signaling, such as farnesyltransferase inhibitors.

The generation of Nf1 and Nf2 mutant mice of different strains has allowed us to perform an in depth tumor spectrum analysis. We have found there to be significant strain effects in the tumor spectrum of F1 mice. This analysis in combination with data collected during aging studies will be crucial to identifying genes that act as dominant modifiers of Nf1 and Nf2. Recently our laboratory discovered a mouse model for astrocytoma. Characterization of the astrocytoma mouse model has revealed the presence of a range of astrocytoma stages and may accurately model human secondary glioblastoma. This mouse model represents the first reported mouse model of astrocytoma initiated by loss of tumor suppressors, rather than overexpression of transgenic oncogenes.

We have taken a variety of biochemical approaches to our characterization of merlin. Purification of a Rac-1 dependent kinase that phosphorylates merlin and the generation of conditional expression systems in cells deficient in Nf2 have been performed. Cell lines that conditionally express merlin will be used to assess Nf2 function in growth control, tumor suppression, and cell survival. After a great deal of testing for optimal conditions, we have designed an in vitro kinase assay that will allow us to purify the protein responsible for merlin regulation. Our data in conjunction with the work of Andrea McClatchey, characterizing the Rac-1/merlin signal transduction pathway, will allow us to better understand the function of Nf2 in human disease.

References

1. K. Cichowski et al., *Science* **286**, 2172-2176 (1999).
2. K. Reilly et al., *Nature Genetics* **26**, 109-113 (2000).
3. R. Shaw et al., *J. Biol. Chem.* **273**, 7757-7764 (1998).
4. D. No et al., *PNAS.* **93**, 3346-51 (1996).
5. Giovannini et al., *Genes and Development.* **14**, 1617-1630 (2000).
6. N.E. Kohl et al., *Methods Enzymol* **255**, 378-386 (1995).
7. N.E. Kohl et al., *Nat Med* **1**, 792-797 (1995).

THE JOURNAL OF BIOLOGICAL CHEMISTRY
Vol. 273, No. 13, Issue of March 27, pp. 7757–7764, 1998
Printed in U.S.A.

Regulation of the Neurofibromatosis Type 2 Tumor Suppressor Protein, Merlin, by Adhesion and Growth Arrest Stimuli*

(Received for publication, August 29, 1997, and in revised form, December 12, 1997)

Reuben J. Shaw, Andrea I. McClatchey‡, and Tyler Jacks§¶

From the Center for Cancer Research and Department of Biology, and §Howard Hughes Medical Institute, Massachusetts Institute of Technology, Cambridge, Massachusetts 02139

The neurofibromatosis type 2 tumor suppressor gene is inactivated in the development of familial and sporadic schwannomas and meningiomas. The encoded protein, Merlin, is closely related to the Ezrin, Radixin, and Moesin family of membrane/cytoskeletal linker proteins. Examination of Merlin in several cell lines revealed that the protein migrates as two distinct species near 70 kDa. Phosphatase treatment and orthophosphate labeling demonstrated that the species with decreased mobility is phosphorylated. Given Merlin's localization to cortical actin structures, we examined the effect of cell-cell contact or other forms of growth arrest on Merlin expression and post-translational modification. Under conditions of confluency or serum deprivation, the levels of phosphorylated and unphosphorylated Merlin species increased significantly. Cells arrested in G_1 by other methods or other phases of the cell cycle did not show changes in Merlin levels. Furthermore, loss of adhesion resulted in a nearly complete dephosphorylation of Merlin, which was reversed upon re-plating of cells, suggesting Merlin phosphorylation may be responsive to cell spreading or changes in cell shape. Thus, the tumor suppressor function of Merlin may involve the regulation of cellular responses to cues such as cell-cell contact, growth factor microenvironment, or changes in cell shape.

Neurofibromatosis type II (NF2)[1] is an autosomal dominant cancer disorder characterized by the development of bilateral schwannomas of the eighth (auditory) cranial nerve. Other features of the disease are spinal nerve root schwannomas and cranial meningiomas (1). Genetic mapping and positional cloning led to the identification of the *NF2* tumor suppressor gene, which was shown to be mutated in the germ line of NF2 patients and in sporadically occurring tumors of the type associated with the disease (2–4).

The *NF2* gene encodes a 595-amino acid protein belonging to the band 4.1 protein superfamily (3, 4). The *NF2*-encoded protein is most similar to three closely related genes in this family, Ezrin, Radixin, and Moesin (the "ERMs") and was hence dubbed Merlin for moesin, ezrin, radixin-like protein. Merlin is most similar to the ERMs in its N-terminal half (*e.g.* 61% identity to Ezrin), whereas the C-terminal half of the protein shares only 24% identity with the other members of this subfamily. *NF2* is transcribed at moderate levels in most human and mouse tissues and is highly expressed in the mouse fetal brain (3–6).[2]

Several members of the band 4.1 superfamily, including the ERM proteins, are thought to serve as membrane-cytoskeletal linkers. Band 4.1 itself is a major component of the erythrocyte undercoat and binds to the integral membrane protein glycophorin C through its N-terminal domain and to actin via spectrin with the C-terminal domain (7). All three of the ERM proteins localize similarly to cortical actin structures near the plasma membrane such as microvilli, membrane ruffles, and lamellipodia (8–12), and each can bind to the integral membrane protein CD44 via their N terminus (13, 14) and to F-actin via their C terminus (15, 16). The proposed actin-binding domain is highly conserved among the ERM proteins, but, importantly, it is not apparent in Merlin. Furthermore, it not known whether Merlin can bind any of the known ERM interactors nor have any novel Merlin binding partners been identified yet.

Depletion of ERM proteins by antisense oligonucleotide treatment, as well as experiments overexpressing Ezrin in insect cells, suggests a role for ERM proteins in regulating cell-substratum and cell-cell adhesion (17, 18); a possible function for Merlin in regulating adhesion has also been reported (19). Additionally, studies of ERM proteins suggest they may serve to reorganize the actin cytoskeleton in response to growth factors (20). Because loss of NF2 function is associated with tumorigenesis and its localization to cortical actin (21–23),[3] we were interested in whether Merlin may be involved in responding to cell-cell contact, loss of substrate attachment, and other growth suppressive signals. Here, we examine the expression of Merlin under such conditions and find the protein is regulated in multiple ways during cellular response to microenvironmental changes.

EXPERIMENTAL PROCEDURES

Cell Culture and Arrest Treatment—NIH3T3 cells (American Type Culture Collection, Rockville, MD) were maintained in Dulbecco's minimum essential medium (DMEM) supplemented with 10% calf serum (Hyclone, Logan, UT). U2OS cells (a gift of J. Lees, Massachusetts Institute of Technology, Cambridge, MA) and NRK cells (a gift of R. Hynes, Massachusetts Institute of Technology, Cambridge, MA) were maintained in DMEM with 10% fetal bovine serum (Hyclone). For serum starvation of cells, subconfluent cells were placed in 0.5% fetal

* This work was supported in part by a grant from the Department of Defense. The costs of publication of this article were defrayed in part by the payment of page charges. This article must therefore be hereby marked "*advertisement*" in accordance with 18 U.S.C. Section 1734 solely to indicate this fact.

‡ Supported by fellowships from the National Neurofibromatosis Foundation and the Medallion Foundation and is currently a recipient of a Burroughs-Wellcome Career award. Present address: Massachusetts General Hospital Cancer Center and Harvard Medical School, Dept. of Pathology, Charlestown, MA 02129.

¶ Associate Investigator of the Howard Hughes Medical Institute. To whom correspondence should be addressed. Tel.: 617-253-0262; Fax: 617-253-9863; E-mail: tjacks@mit.edu.

[1] The abbreviations used are: NF2, neurofibromatosis type II; DMEM, Dulbecco's minimum essential medium; PBS, phosphate-buffered saline; ES, embryonic stem; CCD, cytochalasin D; CIP, calf intestinal phosphatase; NRK, normal rat kidney.

[2] A. I. McClatchey, unpublished observations

[3] R. J. Shaw, A. I. McClatchey, and T. Jacks, submitted for publication.

bovine serum (0.2% calf serum for NIH3T3 cells) for 24 h except where indicated otherwise. For other growth arrest treatments, subconfluent cells in 10% serum were treated with 20 nM staurosporine, 750 μM hydroxyurea (Sigma) for 24 h, 500 ng/ml nocodazole (Sigma) for 24 h, or 500 centigrays γ-irradiation and then placed at 37 °C for 18 h. For confluency experiments, exponentially growing cells were plated at various densities (as noted in figure legends) in fresh medium 24 h before Western lysates were prepared. All cells were cultured in 10-cm tissue culture dishes, and we determined that the saturation density of the NIH3T3 cells used on these dishes was 6×10^6 cells per dish. All cells were incubated at 37 °C under 5% CO_2 in a humidified chamber.

Antibodies—Anti-Merlin polyclonal antibodies sc331 and sc332 were purchased from Santa Cruz Biotechnology (Santa Cruz, CA). Ellen Zwartoff (Erasmus University, Rotterdam, Netherlands) kindly supplied the 1398 Merlin polyclonal antibody (den Bakker *et al.* (21)). All three of these Merlin antisera are anti-peptide polyclonal antibodies directed against unique peptide antigens. sc331, sc332, and 1398 were directed against residues 2–21, 579–579, and 508–533, respectively, of human Merlin. Affinity-purified polyclonal antibody to Radixin (polyclonal antibody 457) was a generous gift of F. Solomon (Massachusetts Institute of Technology, Cambridge, MA) Anti-src MAb (LA074) was a gift of E. Clark (Massachusetts Institute of Technology, Cambridge, MA).

Immunoblotting—Total cell lysates were obtained by two different methods with the same results observed with each methodology. Cultured cells were washed once with PBS and lysed in PBS containing 2% SDS, 0.5 mM phenylmethylsulfonyl fluoride, and 1 μg/ml each aprotinin, leupeptinin, and pepstatin (51); or lysed in boiling 10 mM Tris, pH 7.5, 1% SDS, 50 mM NaF, 1 mM sodium orthovanadate. Cells were then scraped with a rubber policeman, boiled for 5 min, and then sheared with a 26-gauge needle three times, and an aliquot was taken for protein concentration determination using the Bio-Rad DC-Kit (Melville, NY) or using the BCA protein determination kit (Pierce) with identical results. Sample buffer (5 ×) was added to the remainder of the sample.

For immunoblotting, total cell extracts were separated on a 6% SDS-polyacrylamide gel with a 4% stack and electrophoretically transferred to polyvinylidene difluoride membranes (Schleicher & Schuell). For blotting with anti-Merlin sc331, membranes were blocked for 2 h at room temperature with 5% nonfat dry milk in TBST (10 mM Tris, pH 7.5, 150 mM NaCl, 0.05% Tween 20). sc331 was diluted to a final concentration of 1 μg/ml in blocking buffer and incubated overnight at 4 °C. Polyclonal antibody 457 was used as described previously (12). Each was washed extensively in TBST followed by probing with horseradish peroxidase-conjugated anti-mouse or anti-rabbit secondary antibodies (Amersham Corp.) and visualized by enhanced chemiluminescence (Amersham Corp.).

Immunoprecipitation—For methionine labeling, 1×10^6 cells were plated in a 100-mm dish, and the next day the cells were serum-starved (as described above) for 42 h. Cells were then preincubated with 5 ml of methionine-free DMEM (Life Technologies, Inc.) for 40 min and then labeled for 6 h with 500 μCi of [^{35}S]methionine (NEN Life Science Products). For orthophosphate labeling, serum-starved cells were preincubated with phosphate-free DMEM (Life Technologies, Inc.) and then incubated for 5 h with 1 mCi of [^{32}P]orthophosphate (HCl-free, NEN Life Science Products). Cells were rinsed in PBS and then lysed in a modified RIPA buffer (10 mM Tris, pH 7.5, 0.5% sodium deoxycholate, 0.5% Nonidet P-40, 5 mM sodium orthovanadate, 50 mM NaF, 150 mM NaCl, 2 mM EDTA, 0.1% SDS, 1 mM phenylmethylsulfonyl fluoride, 5 μg/ml each of aprotinin, pepstatin, and leupeptin). Lysed cells were rocked at 4 °C for 30 min, then scraped and cleared by centrifugation at top speed in an Eppendorf centrifuge for 15 min. Supernatants were preincubated with irrelevant rabbit IgG in 50% protein A-Sepharose beads (Pierce) at 4 °C for 2 h and then centrifuged for 1 min in an Eppendorf microcentrifuge. The resulting supernatant was used for immunoprecipitation with 0.5 μg of sc331 or sc332 antibody (per sample) overnight at 4 °C. 50 μl of protein A-Sepharose was added and rocked 2 h further at 4 °C. Immunocomplexes were recovered by centifugation and washed three times in RIPA buffer; sample buffer was added, and samples were boiled 5 min. Equal number of trichloroacetic acid-precipitable counts were immunoprecipitated for each sample within a given experiment. Samples were electrophoresed on SDS-polyacrylamide gel electrophoresis as described above.

Flow Cytometry—Flow cytometry analysis was performed using a FACScan (Becton Dickinson). Cells were trypsinized, washed in media, rinsed in PBS, and fixed with cold 95% ethanol. Cells were pelleted and resuspended in 20 μg/ml propidium iodide and 200 μg/ml RNase A in PBS and then incubated at 37 °C for 30 min and placed at 4 °C overnight. A total of 10,000 cells were analyzed for each arrest sample per experiment.

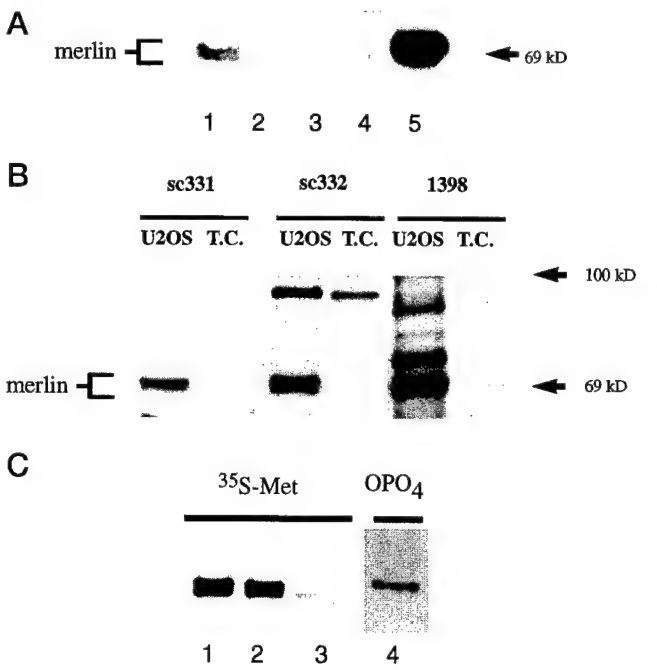

FIG. 1. **Merlin migrates as a doublet near 70 kDa due to differential phosphorylation.** *A*, characterization of sc331 polyclonal antibody to Merlin by immunoblotting. Total cell lysates were made from various cells and immunoblotted as described under "Experimental Procedures." *Lane 1*, wild-type ES cells; *lane 2*, Nf2-deficient (−/−) ES cells; *lanes 3* and *4*, two different tumor cell lines derived from tumors of an *Nf2+/−* mouse that has lost the wild-type Nf2 allele; *lane 5*, NIH3T3 cells transiently overexpressing full-length Merlin cDNA. *B*, characterization of Merlin by immunoprecipitation using three anti-Merlin antibodies. Near-confluent plates of U2OS cells or an Nf2-deficient tumor cell line (*T.C.*) was lysed in a modified RIPA buffer and subjected to immunoprecipitation using the sc331, sc332, or 1398 polyclonal antibodies. Note that all three detect a doublet of approximately 70 kDa that is not detected in the Merlin-deficient tumor cells. Equal numbers of trichloroacetic acid-precipitable counts were immunoprecipitated from each sample. *C*, examination of the phosphorylation status of Merlin. Serum-starved U2OS cells were [^{35}S]methionine-labeled and lysates immunoprecipitated with anti-Merlin sc331 polyclonal antibody. Immunoprecipitates were divided into equal fractions for CIP treatment. *Lane 1*, No treatment; *lane 2*, 0 units of CIP added in CIP buffer and incubated at 30 °C for 1 h; *lane 3*, 1 unit of CIP added and incubated at 30 °C for 1 h; *lane 4*, immunoprecipitate from [lqsb][^{32}P]orthophosphate-labeled 48-h serum-starved U2OS cells. Note that when resolved on the same gel as in *lanes 1–3*, the ^{32}P-labeled Merlin migrates as a single band at the position of the upper species in the ^{35}S-labeled samples. Results shown are representative of four independent experiments.

Phosphoamino Acid Analysis—The phosphoamino acid composition was analyzed essentially as described (52). Briefly, [^{32}P]orthophosphate-labeled immunoprecipitates were separated on a 6% SDS-polyacrylamide electrophoresis gel and transferred to polyvinylidene difluoride as described. Bands containing ^{32}P-labeled Merlin were located by autoradiography, excised, and subjected to direct hydrolysis in 100 μl of 6 N HCl at 100 °C for 1 h. Supernatants were lyophilized and resuspended in distilled H_20 and spotted onto plastic-backed cellulose thin layer chromatography plates (EM Sciences, Gibbstown, NJ). A mixture of 3 mg/ml phosphoserine, phosphothreonine, and phosphotyrosine (Sigma) containing a trace of phenol red was spotted on top of each sample. Two-dimensional high voltage TLC electrophoresis was performed at 1000 V for 20 min each on a Multiphor II (Pharmacia) electrophoretic apparatus. Buffers and visualization of standards were as described (50).

Adhesion Assays—For adhesion assays, confluent NIH3T3 cells were serum-starved in DMEM (0% calf serum) for 18 h, washed with PBS, and trypsinized. Cells were then washed twice in DMEM containing 0.5% soybean trypsin inhibitor and 0.1% bovine serum albumin (essentially fatty acid-free, Sigma) and suspended in DMEM for 30 min at 37 °C. Samples were plated on fibronectin (Biocoat dishes, Becton Dickinson) or tissue culture plastic plates for 15–60 min, except where

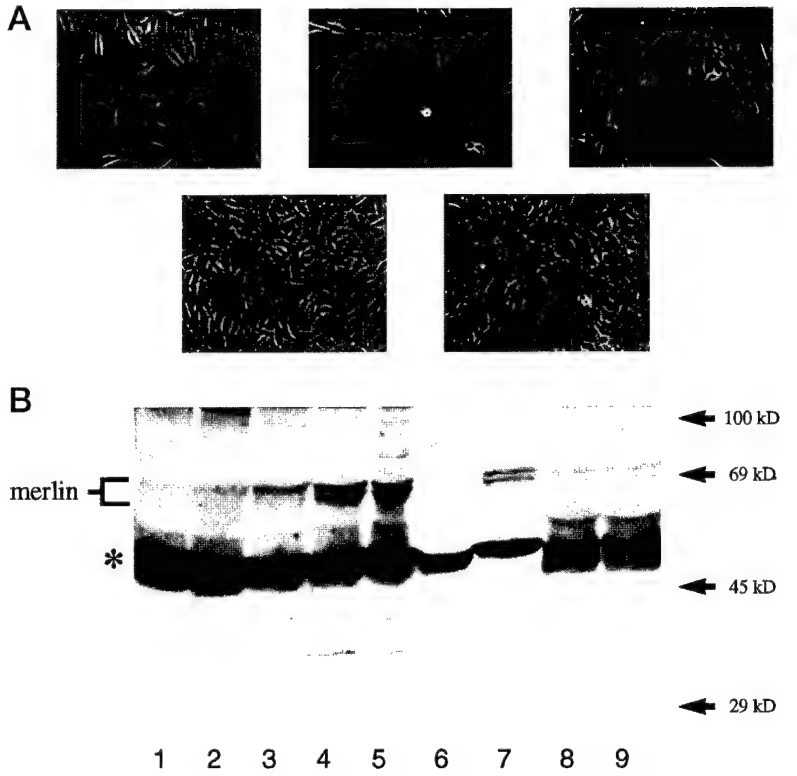

FIG. 2. **Increased confluency and serum deprivation lead to up-regulation of both phosphorylated and unphosphorylated Merlin, with the unphosphorylated form most tightly associated with the arrest.** *A*, phase contrast images of NIH3T3 cells plated at various states of confluency and used for immunoblotting in *lanes 1–5* of *B*. Densities plated are as follows: *1st panel*, 0.25×10^6/10-cm dish; *2nd panel*, 0.5×10^6; *3rd panel*, 1×10^6; *4th panel*, 2×10^6; *5th panel*, 4×10^6. *B*, sc331 immunoblot of total cell lysates from NIH3T3 cells plated at densities shown in *A* (*lanes 1–5*), lysate from Nf2-deficient tumor cells (*lane 6*); 48-h serum-starved NIH3T3 cells (*lane 7*); 48-h serum-starved NIH3T3 cells 5 min following readdition of 10% serum (*lane 8*); 48-h serum-starved NIH3T3 cells 15 min following serum readdition (*lane 9*). *Lanes 7–9* were from plates seeded with 0.5×10^6 cells. Merlin is indicated at *left*. Note the cross-reacting background band (*) demonstrating equivalent loading of protein. Molecular size standards are shown at the *right*. Results shown are representative of five independent experiments.

otherwise indicated. For cytochalasin D (CCD) experiment, CCD was added to 1 μM in DMEM at the time of plating. Similarly for experiments in presence of serum, calf serum was added to 10% in DMEM at time of plating. All plates were washed with PBS prior to making protein extracts to ensure that only adherent cells were examined.

RESULTS

Endogenous Merlin Is Differentially Phosphorylated—To begin to investigate the expression and post-translational modification of Merlin, we characterized the ability of multiple antisera to recognize endogenous Merlin by immunoprecipitation and immunoblotting of total cell lysates. As shown in Fig. 1*A*, Western blot analysis revealed that in mouse embryonic stem (ES) cells the endogenous protein migrated as a distinct doublet around 70 kDa. The identity of these species as Merlin was confirmed by using multiple antisera, cells overexpressing hemagglutinin-tagged Merlin, Nf2-deficient cells derived from tumors from *Nf2*-heterozygous mutant mice, and ES cells bearing a homozygous disruption of the *Nf2* gene (Fig. 1*A*; Ref. 24).

As Merlin had been previously reported to be a phosphoprotein (25), we were interested in whether the nature of the two migrating species was due to phosphorylation. We first characterized the ability of three polyclonal antisera (directed at three distinct peptide epitopes; see "Experimental Procedures") to immunoprecipitate Merlin. Because preliminary experiments indicated that these antisera were more efficient in immunoprecipitating Merlin from human as opposed to mouse cells, human osteosarcoma U2OS cells were employed. As shown in Fig. 1*B*, Merlin was immunoprecipitated as a doublet around 70 kDa in [^{35}S]methionine metabolically labeled U2OS cell lysates by all three antibodies. We also detected two species in immunoprecipitates from mouse, although the two species of human Merlin migrate more closely together (also observed in immunoblot analysis, not shown). Importantly, no immunoreactivity was observed in Merlin-deficient tumor cells (Fig. 1*B*), confirming the specificity of these antibodies.

To address directly the nature of the difference between the two Merlin isoforms, lysates from U2OS cells were immunoprecipitated with the sc331 antibody, and aliquots were treated with calf intestinal phosphatase (CIP). As shown in Fig. 1*C*, CIP treatment eliminated the slower migrating species (*lane 3*), whereas CIP buffer alone had no effect (*lane 2*). More significantly, immunoprecipitation of Merlin from parallel dishes of [^{32}P]orthophosphate-labeled cells yielded a single species, which migrated with the same mobility as the slower form in the ^{35}S-labeled immunoprecipitates (Fig. 1*C*, *lane 4*). A faster migrating species was never observed in any ^{32}P-labeled immunoprecipitates, even upon exposure times 200 times that shown in *lane 4* of Fig. 1*C*. These data demonstrate that the two Merlin species are differentially phosphorylated, with the slower migrating form representing a phosphorylated species and the faster migrating form most likely a fully unphosphorylated form.

Up-regulation of Merlin by Serum Starvation and Confluency—Given Merlin's localization to the cell periphery and its status as tumor suppressor, we were interested in whether the regulation of the protein might be affected by cell-cell contact, which can result in growth inhibition of untransformed cells, as first described in NIH3T3 cells (26). NIH3T3 cells were plated at increasing degrees of confluency (Fig. 2*A*), and Merlin levels were examined by immunoblotting of total cell lysates normalized for total protein levels. As shown in Fig. 2*B*, *lanes 1–5*, with increasing confluency, the levels of both the phosphorylated and unphosphorylated Merlin species increased, with the faster migrating, unphosphorylated form of the protein being most prominent when the majority of the cells in the population had established cell-cell contact (Fig. 2*A*). To examine the specificity of the response, we then determined whether other cell cycle arrest-inducing agents might up-regulate Merlin levels. We first utilized serum starvation to induce quiescence in subconfluent NIH3T3 cells (same density as in Fig. 2*A*, *2nd panel*) and, once again, observed the up-regulation of both phosphorylated and unphosphorylated Merlin species to approximately equimolar amounts (*lane 7*). Strikingly, restimulation of the serum-starved cells resulted in a rapid disappearance of the unphosphorylated form of the protein as follows: within 5–15 min following serum readdition, only a fraction of the faster

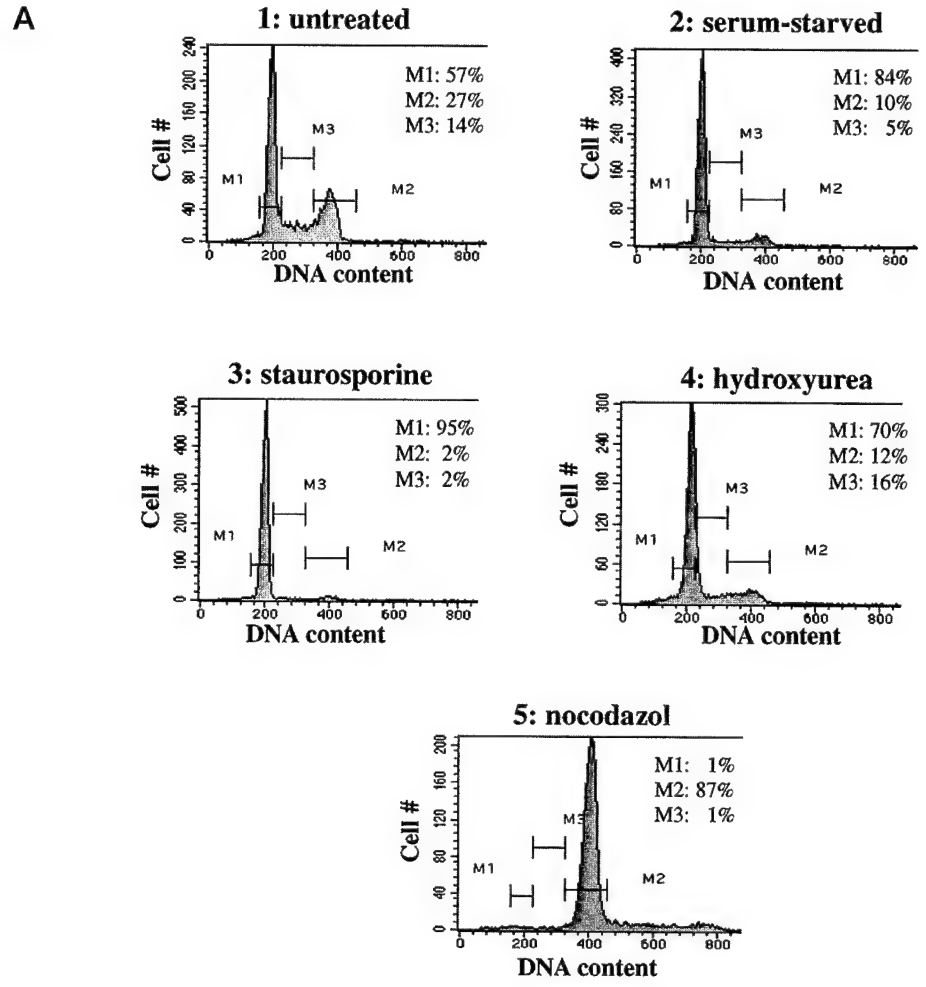

FIG. 3. **Merlin is not up-regulated by other G_1 or cell cycle arrests.** *A*, DNA profiles of cells using propidium iodide and fluorescent activated cell sorter analysis of NIH3T3 cells fixed 24 h following indicated treatments. 1×10^6 cells were plated for each sample. *Panel 1*, untreated cells; *panel 2*, serum-starved in 0.2% calf serum; *panel 3*, 20 nM of staurosporine; *panel 4*, 500 μg/ml nocadazol; *panel 5*, 750 μM hydroxyurea. A total of 10,000 cells were counted for each sample. *M1* represents the percentage of cells found in the G_1 phase of the cell cycle. *M2* represents the G_2/M fraction, and *M3* represents the percentage of cells in S phase. *B*, immunoblot using sc331 antibody of total cell lysates from duplicate cells from treatments in *A*.

migrating form remained (Fig. 2*B*, *lanes 8* and *9*). The level of the phosphorylated, slower migratory species also appeared to decrease modestly following restimulation with 10% serum (Fig. 2*B*, *lanes 7–9*). These results were confirmed using a second polyclonal antibody (1398) (data not shown).

Given that both serum starvation and confluency cause an arrest in the G_0/G_1 phase of the cell cycle, we were interested in whether Merlin levels or phosphorylation status might be affected by growth arrest stimuli generally, or only G_1-specific arrests, or if this response was specific to serum deprivation and confluency. To address this question, duplicate sets of sparsely plated NIH3T3 cells were treated with a variety of growth-suppressive agents or were left untreated for 24 h. One set was then subjected to cell cycle characterization utilizing propidium iodide labeling and fluorescent activated cell sorter analysis (Fig. 3*A*). Total cell extracts were made from the other set of plates, equilibrated for total protein, and immunoblotted as before (Fig. 3*B*). While serum deprivation for 24 h led to a significant increase in protein levels, no up-regulation of phosphorylated or unphosphorylated Merlin was observed in cells treated with another G_1 arresting agent, staurosporine (Fig. 3*B*, *3rd lane*) (27). Furthermore, no up-regulation of Merlin was

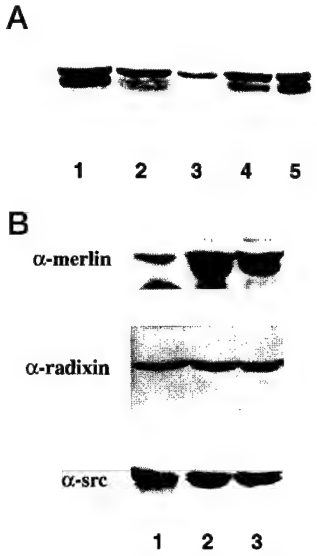

FIG. 4. **Up-regulation of Merlin is not specific to NIH3T3 cells; Radixin is also regulated by confluency.** *A*, sc331 immunoblot of total cell lysates from NRK cells plated at the following densities in a 10-cm dish with any treatment indicated: *lane 1*, 1×10^6 cells serum-starved for 48 h; *lane 2*, 1×10^6 cells starved 48 h and 15 min following 10% serum readdition; *lane 3*, 0.5×10^6 cells; *lane 4*, 2×10^6 cells; *lane 5*, 4×10^6 cells. *B*, immunoblot of total cell lysates from NIH3T3 cells at various densities using anti-Merlin (sc331), anti-Radixin, and anti-src antibodies. *Lane 1*, 0.5×10^6 cells; *lane 2*, 2.5×10^6 cells; *lane 3*, 4×10^6 cells.

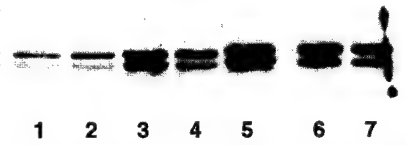

FIG. 5. **Serum deprivation synergizes with the effects of confluency.** sc331 immunoblot of total cell lysates from NIH3T3 cells plated at indicated densities with noted treatments: *lane 1*, 0.25×10^6 cells; *lane 2*, 1×10^6 cells; *lane 3*, 4×10^6 cells; *lane 4*, 4×10^6 cells stimulated for 15 min with 10% serum; *lane 5*, 4×10^6 cells serum-starved; *lane 6*, 6×10^6 cells; *lane 7*, 6×10^6 cells stimulated for 15 min with 10% serum.

observed in cells treated with γ-irradiation, nocodazole, or hydroxyurea (Fig. 3*B*, *4th* and *5th lanes*; data not shown). As shown in Fig. 3*A*, hydroxyurea and nocodazole led to early S phase and G_2/M arrest, respectively. Similar results were obtained with U2OS cells (data not shown). Thus, the changes in Merlin expression associated with confluency and serum deprivation appear to be specific and not a secondary consequence of a G_1 phase or more general cell cycle arrest.

To investigate whether this was a general property of Merlin regulation or a phenomenon specific to NIH3T3 cells, we examined many cell types from different species, including murine embryonic and Rat1 fibroblasts, normal rat kidney (NRK), and human osteosarcoma (MG63 and U20S) cells (Fig. 4*A* and data not shown). In all cell types examined, both confluency and serum starvation were associated with the presence of the two migrating forms of Merlin, of which the faster species was diminished upon addition of serum or in low density cells. To examine whether this form of regulation was specific to Merlin, we stripped and reprobed the anti-Merlin immunoblot from Fig. 4*B* (of NIH3T3 total cell lysates) with an anti-Radixin polyclonal antibody (12). Radixin was also up-regulated by confluency but did not migrate as two distinct species (Fig. 4*B*). We determined that there was no cross-reactivity of the Radixin antibody for Merlin. Serum starvation/restimulation did not affect Radixin levels or mobility (data not shown). These same lysates were run in parallel and probed with an anti-c-*src* antibody, which confirmed that equivalent amounts of protein were loaded in each lane (Fig. 4*B*).

To determine whether the increase in Merlin levels at higher cell confluency might just be due to exhaustion of critical serum factors in the media, we examined whether treating cells plated at high density with fresh serum might reduce Merlin levels. As shown in Fig. 5, cells plated at near-saturation density showed a preferential loss of the unphosphorylated form of Merlin when treated with serum (compare *lanes 3* and *4* of Fig. 5). Importantly, however, the levels of Merlin after serum treatment were still significantly higher than the level in more sparsely plated cells (compare *lane 4* to *lanes 1* and *2* of Fig. 5). These results suggest that confluency and serum deprivation synergize in their up-regulation of Merlin. Consistent with this idea, serum-starvation of the densely plated cells resulted in even further up-regulation of Merlin levels (compare *lanes 3* and *5*, Fig. 5). On the contrary, however, cells plated at saturation density (6×10^6 for our NIH3T3 cells on a 10-cm dish) did not show a loss of Merlin levels when treated with serum, arguing that at the highest cell densities, these cells were no longer responsive to the serum factors that induce down-regulation of Merlin (Fig. 5, *lanes 6* and *7*).

Merlin Is Phosphorylated on Serine and Threonine—To identify which residues are phosphorylated in these cells and to determine if the loss of the unphosphorylated form of Merlin following serum treatment results in the appearance of a novel phosphorylated form, we performed phosphoamino acid analysis on serum-starved and serum-treated U2OS cells. As shown in Fig. 6, Merlin is phosphorylated on both serine and threonine residues but apparently not on tyrosine residues; moreover, the ratio of serine to threonine phosphorylation was not affected by serum treatment.

Merlin Phosphorylation Is Also Regulated by Loss of Adhesion and Cell Spreading—Antisense oligonucleotide experiments have suggested a role for Merlin and the other ERM proteins in regulating cell adhesion (17, 19). Given our results with serum deprivation and confluency, we were interested in whether loss of adhesion might also modulate Merlin protein levels or phosphorylation. To test this idea, total cell lysates were made from serum-starved, confluent NIH3T3 cells before or after trypsinization and placement in suspension in the absence of serum for 30 min (28). As shown in Fig. 7*A*, placement of the cells in suspension resulted in a rapid loss of the phosphorylated form of Merlin and a concomitant increase in the level of unphosphorylated Merlin. Parallel cultures kept in suspension for 30 min were then replated on tissue culture plastic plates in the absence of serum to address whether adhesion might be capable of re-inducing Merlin phosphorylation. Indeed, upon replating, the slower migrating species of Merlin returned, with the ratio of phosphorylated to unphosphorylated reaching nearly one to one at 1 h post-plating (Fig. 7*A*). It should be noted for all of these experiments that the plates were washed prior to preparing total cell lysates, so only adherent cells were collected.

To examine further a possible connection between Merlin regulation and cell shape, cells in suspension were plated on fibronectin in the absence or presence of CCD, which disrupts the actin cytoskeleton. CCD treatment allows for cell attachment but prevents cell spreading (29). Plating of cells on fibronectin resulted in clear phosphorylation of Merlin when compared with suspended cells, but this was prevented when cells were plated in the presence of 1 μM CCD (Fig. 7*B*). Microscopic analysis revealed that the CCD-treated cells were well attached but not spread, as described previously (29).

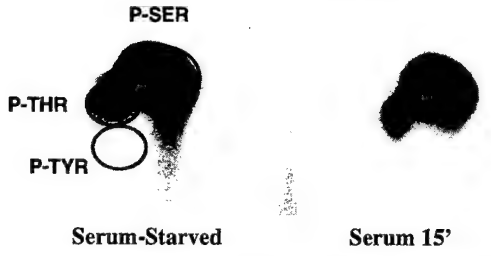

FIG. 6. **Merlin is constitutively phosphorylated on serine and threonine residues.** Phosphoamino acid analysis from serum-starved and serum-stimulated U2OS cells, performed as described under "Experimental Procedures," is shown. Positions of phosphoserine (*P-SER*), phosphothreonine (*P-THR*), and phosphotyrosine (*P-TYR*) standards are indicated.

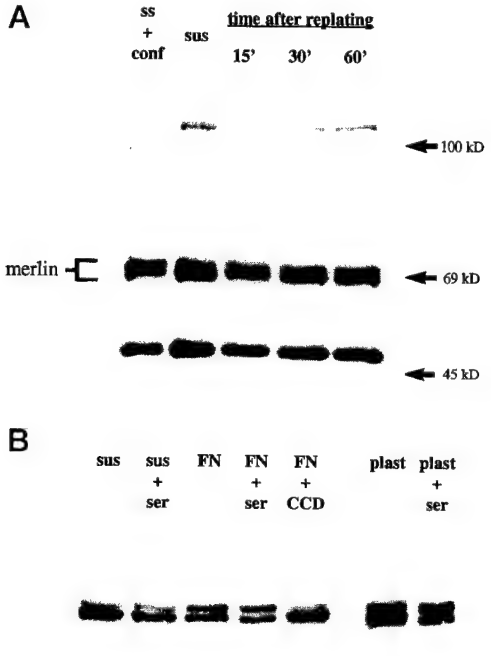

FIG. 7. **Merlin phosphorylation is regulated by cell spreading, which synergizes with growth factor-induced phosphorylation.** *A*, sc331 immunoblot of confluent NIH3T3 cells, serum-starved for 18 h, placed in suspension for 30 min, and then replated on tissue culture plastic plates. Total cell lysates were made prior to suspension (*ss + confl*), after 30 min of suspension (*sus*), or from cells 15, 30, or 60 min after replating. Replated cells were washed with PBS to remove nonadherent cells, and then total cell lysates were prepared. Note: *2nd lane* is overloaded. *B*, sc331 immunoblot of confluent, starved NIH3T3 cells kept in suspension or plated on fibronectin (*FN*) or tissue culture plastic plates (*plast*) in the absence or presence of 10% calf serum (+ *ser*) or 1 μM cytochalasin D (+ *CCD*).

Given the ability of cell spreading to induce Merlin phosphorylation in the absence of serum, we were interested in whether serum factors could have this effect alone on cells in suspension and whether they might synergize with cell spreading to induce Merlin phosphorylation. As shown in Fig. 7*B*, treatment of suspended cells with serum did not result in a significant phosphorylation of Merlin. However, when combined with plating (on fibronectin or tissue culture plastic plates), serum addition led to an enhancement of the phosphorylation of Merlin (Fig. 7*B*). These results suggest that serum factors and cell spreading synergize in regulating the ratio of phosphorylated to unphosphorylated Merlin but that a cell spreading or shape-specific signal is needed in order for Merlin to be responsive to growth factor-mediated phosphorylation.

DISCUSSION

Neurofibromatosis type 2 is a severe inherited cancer disorder that predisposes individuals to bilateral vestibular schwannomas, as well as meningiomas and spinal schwannomas. In 1993, two groups used positional cloning to isolate the *NF2* gene, which has since been found to be mutated in sporadically occurring schwannomas, meningiomas, and malignant mesotheliomas (2). Further supporting a broad role for NF2 in tumor suppression, mice heterozygous for a targeted mutation at the *Nf2* locus are predisposed to a wide range of tumor types.[4]

The *NF2*-encoded protein, Merlin, is structurally related to a group of proposed membrane/cytoskeletal linker proteins, particularly the ERM proteins. However, Merlin has not been shown to be functionally related to these proteins. Moreover, it remains unclear how such a protein may serve to regulate proliferation or how its loss might contribute to tumorigenesis. Key in the early understanding of other important tumor suppressors were studies that examined the expression and post-translational modification of these proteins (*e.g.* cell cycle-dependent phosphorylation of the retinoblastoma protein (30–32) and up-regulation of p53 by DNA damaging agents (33)), which ultimately proved instrumental in pointing the way toward understanding the function of those genes. We and others (21, 23)[3] have demonstrated that Merlin localizes similarly to the ERM proteins at the membrane/actin interface, with Merlin being particularly enriched in membrane ruffles. Given the localization of Merlin to regions of dynamic actin at the cell periphery, and its role as a tumor suppressor, we were interested in whether growth inhibition associated with cell-cell contact might cause a change in the pattern of Merlin expression. We observed that the level of endogenous Merlin protein is increased by confluency as well as by serum deprivation and that the two stimuli can synergize in their up-regulation of Merlin levels. Furthermore, we have discovered that these stimuli are tightly associated with the appearance of a novel, unphosphorylated species of Merlin. This unphosphorylated form disappears rapidly (<5 min) following serum addition to serum-starved cells, suggesting a tight post-translational regulation of this species leading to its rapid degradation by growth factor-activated pathways. The up-regulation of Merlin was not observed in cells arrested in G_1 by staurosporine or in cells arrested in S or G_2/M induced by hydroxyurea or nocodazole, respectively, suggesting that the effects of cell-cell contact and serum deprivation stimuli are specific.

Merlin appears to be constitutively phosphorylated on both serine and threonine residues, and no obvious changes in patterns of phosphorylation were discerned following serum treatment or in confluent *versus* subconfluent conditions (data not shown). The protein was previously reported to be phosphorylated specifically on serine in human U251-MG glioblastoma cells (25). Given the abundant threonine phosphorylation observed in our experiments, it is not clear whether there may be a cell type-specific difference or that the threonine phosphorylation was below the level of detection in the previous experiments. The fact that we detect threonine phosphorylation is of particular interest as a germ line missense mutation of Thr-352 of Merlin has been detected in a severely affected NF2 patient (34), and this residue bears a possible consensus recognition sequence for protein kinase C (3, 35). All three ERM proteins have been shown to be serine/threonine, as well as tyrosine, phosphorylated in response to specific growth factors in various cellular contexts (20, 36, 37), although Merlin lacks almost all

[4] A. I. McClatchey, I. Saotome, K. Mercer, D. Crowley, J. Gusella, R. Bronson, and T. Jacks, submitted for publication.

of the previously described phosphorylation sites found in the other family members. Furthermore, there was no increase in the level of phosphorylation on Merlin following serum treatment (data not shown); it remains to be determined whether individual growth factors might induce phosphorylation of Merlin.

In addition to the regulation of Merlin levels and phosphorylation by serum and confluency, we found that loss of adhesion leads to a rapid, nearly complete dephosphorylation of Merlin. This effect was reversed by replating the cells which led to rephosphorylation of Merlin to control levels. The phosphorylation of Merlin upon replating showed a close correlation with degree of cell spreading, and, in fact, blocking cell spreading by cytochalasin D treatment prevented the phosphorylation effect. Interestingly, experiments using antisense oligonucleotides have demonstrated that loss of ERM proteins leads to a loss of cell-cell and cell-substratum attachment (17), and a similar approach has suggested a role for Merlin in cell-substratum attachment (19). Furthermore, overexpression of Ezrin has been shown to increase the adhesion of insect cells to their substratum and to override contact inhibition of confluent NIH3T3 cells (18, 38). Whether Merlin directly modulates the activity of the ERM proteins in these processes or responds to the same cues that stimulate ERM-mediated cytoskeletal reorganization, but performs a distinct function in regulating proliferation, remains to be determined.

The responsiveness of Merlin to confluency, serum deprivation, and loss of substratum attachment may be due to a common upstream signal regulating the organization of the actin cytoskeleton. It is interesting that other microfilament-associated proteins such as Vinculin, ZO-1, Gas2, and the MARCKS protein are all up-regulated upon confluency and/or serum starvation-induced arrest (39–42), and in fact, Vinculin is regulated by cell shape as well (39). One possible component of the upstream signal could be members of the Rho subfamily of small GTPases. These proteins are known to regulate the actin cytoskeleton as well as mitogenic signaling and cell cycle progression in G_0/G_1 in fibroblasts in response to extracellular signals (43, 44). Intriguingly, the activity of RhoA in Swiss 3T3 cells is reduced by serum deprivation, confluency, and placement of cells into suspension (45–47). The ERM proteins (48) as well as Merlin (49) have been reported to colocalize with RhoA in various cellular contexts, and Rho modulates the affinity of ERM proteins for their membrane targets (14). Moreover, we have recently demonstrated that RhoA activity is necessary and sufficient for the phosphorylation and relocalization of the ERM proteins (50). Perhaps the phosphorylation and/or levels of Merlin are responsive to changes in RhoA activity as well, or alternatively, Merlin may serve to downmodulate the activity of RhoA or a related GTPase in response to these environmental signals.

Although the function of Merlin is still largely unknown, the data presented here represent a first step toward understanding what stimuli may regulate its activity. Taken together, our results suggest Merlin may serve its tumor suppressor role in the response of cells to loss of cell-substratum attachment, increased cell-cell contact, or poor growth factor microenvironment, perhaps preventing inappropriate cell-cycle entry under these circumstances. Furthermore, the unphosphorylated form of the protein may represent the active tumor suppressor conformation. Given that the protein is up-regulated by some growth arrest stimuli, it is possible that Merlin participates in these arrest responses and that loss of Merlin function might lead to loss of growth arrest capacity under certain conditions and, ultimately, to tumor formation. An interesting test of these ideas would be to examine the ability of cells deficient for Merlin to arrest under conditions of confluency, serum deprivation, or growth in suspension.

Acknowledgments—We thank Ichiko Saotome for excellent technical assistance in helping generate and maintain Nf2-deficient ES cells and tumor cells; Ellen Zwartoff and Frank Solomon for kindly supplying antibodies; Karen Cichowski and Michelle Starz for technical advice; and Jimmy Wong for computer assistance.

REFERENCES

1. Martuza, R. L., and Eldrige, R. (1988) *N. Engl. J. Med.* **318,** 684–688
2. Gusella, J. M., Ramesh, V., MacCollin, M., and Jacoby, L. B. (1996) *Curr. Opin. Genet. Dev.* **6,** 87–92
3. Rouleau, G. A., Merel, P., Lutchman, M., Sanson, M., Zucman, J., Marineau, C., Hoang-Xuan, K., Demczuk, S., Desmaze, C., Plougastel, B., Pulst, S., Lenior, P., Bijlsma, E., Fashold, R., Dumanski, J., deJong, P., Parry, D., Eldrige, R., Aurias, A., Delattre, O., and Thomas, G. (1993) *Nature* **363,** 515–521
4. Trofatter, J. A., MacCollin, M. M., Rutter, J. L., Murrell, J. R., Duyao, M. P., Parry, D. M., Eldrige, R., Kley, N., Menon, A. G., Pulaski, K., Haase, V. H., Ambrose, C. A., Munroe, D., Bove, C., Haines, J. H., Martuza, R. L., McDonald, M. E., Seizinger, B. R., Short, M. P., Buckler, A. J., and Gusella, J. F. (1993) *Cell* **72,** 791–800
5. Gutmann, D. H., Wright, D. E., Geist, R. T., and Snider, W. D. (1995) *Hum. Mol. Genet.* **4,** 471–478
6. Huynh, D., Tran, T., Nechiporuk, T., and Pulst, S. (1996) *Cell Growth Differ.* **7,** 1551–1561
7. Luna, E. J., and Hitt, A. L. (1992) *Science* **258,** 955–964
8. Amieva, M., and Furthmayr, H. (1995) *Exp. Cell Res.* **219,** 180–196
9. Berryman, M., Franck, Z., and Bretscher, A. (1993) *J. Cell Sci.* **105,** 1025–1043
10. Franck, Z., Gary, R., and Bretscher, A. (1993) *J. Cell Sci.* **105,** 219–231
11. Sato, N., Funayama, N., Nagafuchi, A., Yonemura, S., Tsukita, S., and Tsukita, S. (1992) *J. Cell Sci.* **103,** 131–143
12. Winckler, B., Gonzalez Agosti, C., Magendantz, M., and Solomon, F. (1994) *J. Cell Sci.* **107,** 2523–2534
13. Tsukita, S., Oishi, K., Sato, N., Sagara, J., Kawai, A., and Tsukita, S. (1994) *J. Cell Biol.* **126,** 391–401
14. Hirao, M., Sato, N., Kondo, T., Yonemura, S., Monden, M., Sasaki, T., Takai, Y., Tsukita, S., and Tsukita, S. (1996) *J. Cell Biol.* **135,** 37–51
15. Pestonjamasp, K., Amieva, M. R., Strassel, C. P., Nauseef, W. M., Furthmayr, H., and Luna, E. J. (1995) *Mol. Biol. Cell* **6,** 247–259
16. Turunen, O., Wahlstrom, T., and Vaheri, A. (1994) *J. Cell Biol.* **126,** 1445–1453
17. Takeuchi, K., Sato, N., Kasahara, H., Funayama, N., Nagafuchi, A., Yonemura, S., Tsukita, S., and Tsukita, S. (1994) *J. Cell Biol.* **125,** 1371–1384
18. Martin, M., Andreoli, C., Sahuquet, A., Montcourrier, P., Algrain, M., and Mangeat, P. (1995) *J. Cell Biol.* **128,** 1081–1093
19. Huynh, D. P., and Pulst, S. M. (1996) *Oncogene* **13,** 73–84
20. Bretscher, A. (1989) *J. Cell Biol.* **108,** 921–930
21. den Bakker, M. A., Riegman, P. H., Hekman, R. A., Boersma, W., Janssen, P. J., van der Kwast, T. H., and Zwarthoff, E. C. (1995) *Oncogene* **10,** 757–763
22. McCartney, B. M., and Fehon, R. G. (1996) *J. Cell Biol.* **133,** 843–852
23. Gonzalez-Agosti, C., Xu, L., Pinney, D., Beauchamp, R., Hobbs, W., Gusella, J., and Ramesh, V. (1996) *Oncogene* **13,** 1239–1247
24. McClatchey, A. I., Saotome, I., Ramesh, V., Gusella, J. F., and Jacks, T. (1997) *Genes Dev.* **11,** 1253–1265
25. Takeshima, H., Izawa, I., Lee, P. S., Safdar, N., Levin, V. A., and Saya, H. (1994) *Oncogene* **9,** 2135–2144
26. Fisher, H. W., and Yeh, J. (1967) *Science* **155,** 581–582
27. Crissman, H. A., Gadbois, D. M., Tobey, R. A., and Bradbury, E. M. (1991) *Proc. Natl. Acad. Sci. U. S. A.* **88,** 7580–7584
28. Clark, E. A., and Hynes, R. O. (1996) *J. Biol. Chem.* **271,** 14814–14818
29. Zhu, X., and Assoian, R. K. (1995) *Mol. Biol. Cell* **6,** 273–282
30. DeCaprio, J., Ludlow, J., Lynch, D., Furukawa, Y., Griffin, J., Pinica-Worms, H., Huang, C., and Livingston, D. (1989) *Cell* **58,** 1085–1095
31. Bukanovich, K., Duffy, L., and Harlow, E. (1989) *Cell* **58,** 1097–1105
32. Chen, P. L., Scully, P., Shew, J., Wang, J., and Lee, W. H. (1989) *Cell* **58,** 1193–1198
33. Maltzan, W., and Czyzyk, L. (1984) *Mol. Cell. Biol.* **4,** 1689–1694
34. Bourn, D., Carter, S. A., Mason, S., Gareth, D., Evans, R., and Strachan, T. (1994) *Hum. Mol. Genet.* **3,** 813–816
35. Kennelly, P. J., and Krebs, E. G. (1991) *J. Biol. Chem.* **266,** 15555–15558
36. Fazioli, F., Wong, W. T., Ullrich, S. J., Sakaguchi, K., Appella, E., and Di Fiore, P. P. (1993) *Oncogene* **8,** 1335–1345
37. Nakamura, F., Amieva, M. R., and Furthmayr, H. (1995) *J. Biol. Chem.* **270,** 31377–31385
38. Kaul, S. C., Mitsui, Y., Komatsu, Y., Reddel, R. R., and Wadhwa, R. (1996) *Oncogene* **13,** 1231–1237
39. Ungar, F., Geiger, B., and Ben-Ze'ev, A. (1986) *Nature* **319,** 787–791
40. Brancolini, C., and Schneider, C. (1994) *J. Cell Biol.* **124,** 743–756
41. Herget, T., Brooks, S. F., Broad, S., and Rozengurt, E. (1993) *Proc. Natl. Acad. Sci. U. S. A.* **90,** 2945–2949
42. Gottardi, C. J., Arpin, M., Fanning, A. S., and Louvard, D. (1996) *Proc. Natl. Acad. Sci. U. S. A.* **93,** 10779–10784
43. Ridley, A. J. (1996) *Curr. Biol.* **6,** 1256–1265
44. Machesky, L. M., and Hall, A. (1996) *Trends Cell Biol.* **6,** 304–310
45. Ridley, A. J., and Hall, A. (1992) *Cell* **70,** 389–399

46. Paterson, H. F., Self, A. J., Garrett, M. D., Just, I., Aktories, K., and Hall, A. (1990) *J. Cell Biol.* **111,** 1001–1007
47. Chong, L. D., Traynor-Kaplan, A., Bokoch, G. M., and Schwartz, M. A. (1994) *Cell* **79,** 507–513
48. Takaishi, K., Sasaki, T., Kameyama, T., Tsukita, S., Tsukita, S., and Takai, Y. (1995) *Oncogene* **11,** 39–48
49. Scherer, S. S., and Gutmann, D. H. (1996) *J. Neuro. Res.* **46,** 595–605
50. Shaw, R. J., Henry, M., Solomon, F., and Jacks, T. (1998) *Mol. Biol. Cell* **9,** 403–419
51. Henry, M. D., Gonzalez Agosti, C., and Solomon, F. (1995) *J. Cell Biol.* **129,** 1007–1022
52. Sefton, B. (1995) *Current Protocols in Molecular Biology*, (Ausubel, F. M., Brent, R., Kingston, R., Moore, D., Seidman, J., Smith, J., and Struhl, K., eds) pp. 18.3.1–18.3.18, John Wiley & Sons, Inc., New York

Reprint Series
10 December 1999, Volume 286, pp. 2172–2176

Science

Mouse Models of Tumor Development in Neurofibromatosis Type 1

Karen Cichowski,[1]* T. Shane Shih,[1,2]* Earlene Schmitt,[1,3] Sabrina Santiago,[1] Karlyne Reilly,[1] Margaret E. McLaughlin,[4] Roderick T. Bronson,[5] and Tyler Jacks[1,6]†

Mouse Models of Tumor Development in Neurofibromatosis Type 1

Karen Cichowski,[1]* T. Shane Shih,[1,2]* Earlene Schmitt,[1,3] Sabrina Santiago,[1] Karlyne Reilly,[1] Margaret E. McLaughlin,[4] Roderick T. Bronson,[5] Tyler Jacks[1,6]†

Neurofibromatosis type 1 (NF1) is a prevalent familial cancer syndrome resulting from germ line mutations in the *NF1* tumor suppressor gene. Hallmark features of the disease are the development of benign peripheral nerve sheath tumors (neurofibromas), which can progress to malignancy. Unlike humans, mice that are heterozygous for a mutation in *Nf1* do not develop neurofibromas. However, as described here, chimeric mice composed in part of $Nf1^{-/-}$ cells do, which demonstrates that loss of the wild-type *Nf1* allele is rate-limiting in tumor formation. In addition, mice that carry linked germ line mutations in *Nf1* and *p53* develop malignant peripheral nerve sheath tumors (MPNSTs), which supports a cooperative and causal role for p53 mutations in MPNST development. These two mouse models provide the means to address fundamental aspects of disease development and to test therapeutic strategies.

Neurofibromatosis type I (NF1) affects about 1 in 3500 individuals worldwide (*1*). The hallmark clinical feature of the disease is development of multiple benign neurofibromas, which can be debilitating, severely disfiguring, and, in some patients, progress to

malignancy (*2*). NF1 patients are also predisposed to developing optic pathway gliomas, pheochromocytomas, and myeloid leukemia as well as several symptoms unrelated to cancer (*3*).

The *NF1*-encoded protein neurofibromin is a member of the GTPase-activating protein (GAP) family that includes mammalian $p120^{GAP}$ and the yeast IRA proteins (*4*). Like $p120^{GAP}$, neurofibromin can stimulate the GTPase activity of Ras in vitro and in vivo (*5*). Because most mutations in the *NF1* gene in patients are predicted to result in loss of function, deregulation of Ras-mediated signaling is likely to contribute to the pathology of NF1 (*6*).

Although *NF1* appears to be a classic tumor suppressor gene, the molecular mechanism underlying tumor development in NF1 has been obscure. Although second hit mutations affecting the inherited wild-type *NF1* allele have been clearly identified in the myeloid leukemias and pheochromocytomas in NF1 patients (*7*), such mutations have been reported for only a small number of neurofibromas (*8*). The difficulty in detecting mutations may be due in part to the complex nature of these lesions, which are composed of multiple cell types, not all of which are expected to develop a second mutation (*2*). However, it also has been suggested that *NF1* heterozygosity may be sufficient for development of benign neurofibromas (haplo-insufficiency), with full loss of *NF1* function being restricted to the progression to MPNSTs (*9*).

Heterozygous mutant ($Nf1^{+/-}$) animals are predisposed to a number of tumor types; however, they do not develop peripheral nerve sheath tumors or other characteristic symptoms of human NF1 (*10, 11*). To test the possibility that a mutation in the wild-type *Nf1* allele is required and rate-limiting in the formation of neurofibromas in $Nf1^{+/-}$ mice, we generated chimeric mice that were partially composed of $Nf1^{-/-}$ cells. Germ line homozygosity for a *Nf1* mutation ($Nf1^{-/-}$) results in embryonic lethality at about day 14 of gestation (*10, 11*). We also developed a model of MPNST formation by generating mice with combined mutations in *Nf1* and *p53*. These two models are described below.

We created two *Nf1*-deficient embryonic stem cell (ES) lines by successive rounds of gene targeting and injected the cells into C57BL/6 blastocysts to generate chimeric mice (*12*). We analyzed 18 chimeric adults, which fell into three phenotypic classes, in this study (*13*). The subset of chimeras (n = 4) that exhibited the highest degree of chimerism died by 1 month of age of unknown causes. The two animals that exhibited the lowest degree of chimerism (less than 15% by coat color) lived a typical life span and no unusual pathology was observed upon necropsy. Most animals (12/18) fell into the third phenotypic class: they exhibited a moderate degree of chimerism, frequent myelodysplasia, and progressive neuromotor defects. The life span of these animals varied from 2 to 26 months. Histological analysis of this subset of mice revealed the presence of neurofibromas in every animal (*14*). We detected mul-

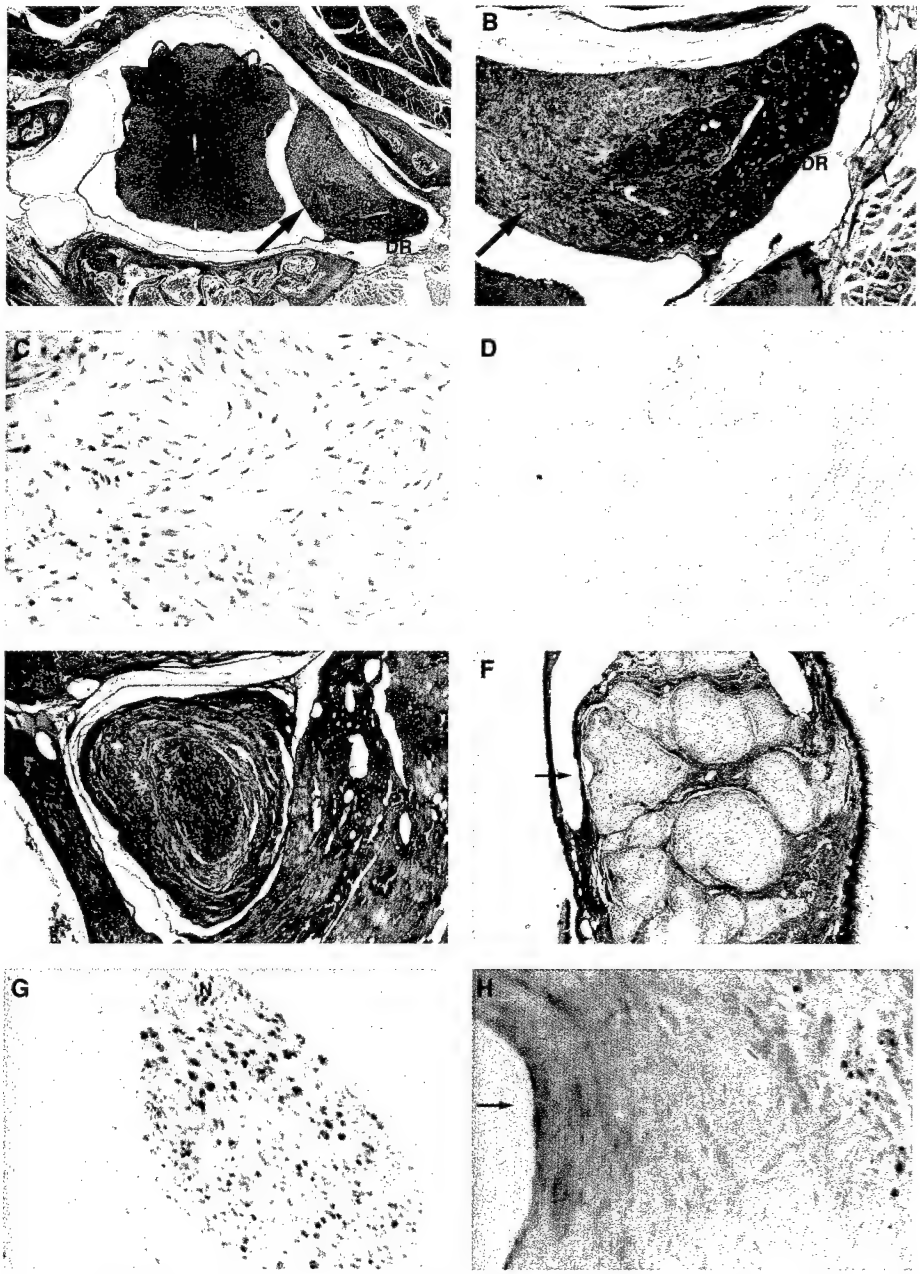

Fig. 1. Histological analysis of neurofibromas from $Nf1^{-/-}$:$Nf1^{+/+}$ chimeras. (**A** and **B**) Sections through the spinal cord (SC) and dorsal root (DR) or limb muscle (**C**) from different $Nf1^{-/-}$:$Nf1^{+/+}$ chimeric mice were stained with H+E. (B) Higher magnification of (A). Arrows in (A) and (B) indicate the neoplastic region. The entire field is composed of neoplastic tissue in (C). (**D**) Tissues from $Nf1^{+/+}$:$Nf1^{-/-}$; *ROSA-26*$^{+/-}$ mice were stained with X-Gal as described in (*31*). Sections of muscle (**E**) and tongue (**F**) were stained with H+E. A nerve (N) is seen in the center of the neurofibroma in (E). The neurofibroma in the tongue shown in (F) is multinodular and a portion of it identified by the arrow is also shown in (H). (**G** and **H**) Sections adjacent to (E) and (F) (higher magnification) were stained with an antibody recognizing the S100 protein.

[1]Department of Biology and Center for Cancer Research and [6]Howard Hughes Medical Institute, Massachusetts Institute of Technology, Cambridge, MA 02139, USA. [2]Merck & Co., Whitehouse Station, NJ 08889, USA. [3]Breast Center, Baylor College of Medicine, One Baylor Plaza, MS 600, Houston, TX 77030, USA. [4]Brigham and Women's Hospital, Department of Pathology, Boston, MA 02115, USA. [5]Department of Pathology, Tufts University Schools of Medicine and Veterinary Medicine, Boston, MA 02111, USA.

*These authors contributed equally to this work.
†To whom correspondence should be addressed. E-mail: tjacks@mit.edu

tiple tumors (10 to 100 per mouse), which usually emanated from the dorsal root ganglia (Fig. 1, A and B) or peripheral nerves in the limbs (Fig. 1C). Notably, only plexiform neurofibromas (those growing along the plexus of internal peripheral nerves) were observed; dermal neurofibromas, which are more common in NF1 patients, were not detected. Histologically, the lesions exhibited the classic features of human neurofibromas (*15*). Most tumors were not visible macroscopically; thus, the number of tumors per animal was probably underestimated. In two chimeras, however, tumors on the trigeminal nerve and in the tongue were visible upon dissection.

The contribution of $Nf1^{-/-}$ cells in the neurofibromas in these mice was assessed by using $Nf1^{-/-}$ ES cells containing a β-galactosidase (β-gal) expressing transgene (*16*). Five chimeras were produced with these cells. Two of the three highly chimeric animals developed multiple neurofibromas. In all cases, near uniform β-gal expression was observed in the tumors, demonstrating extensive contribution of $Nf1^{-/-}$ cells (Fig. 1D). We have not detected significant recruitment of wild-type cells into these lesions as might have been expected given the multicellular nature of human neurofibromas (see below). However, the sensitivity of 5-bromo-4-chloro-3-indolyl β-D-galactopyranoside (X-Gal) staining is not sufficient to rule out a low-level contribution of wild-type cells in this model.

Human neurofibromas contain a variety of cell types found in normal peripheral nerve including Schwann cells, perineurial cells, fibroblasts, and neurons (*15*). We used electron microscopy (EM) to determine the cellular constituents of the lesions in this mouse model. Figure 2A illustrates the overall ultrastructural appearance of a neurofibroma in this model. As in human neurofibromas Schwann cells were the most common cell type present (Fig. 2, B and C). Importantly, Schwann cells (or their precursors) are believed to be the initiating cell type [the cell type that undergoes loss of heterozygosity (LOH)] in human tumors. Cells exhibiting features of perineurial cells were also observed by EM (Fig. 2D). Taken together with the histological analysis, these data demonstrate a close similarity between the lesions in $Nf1^{-/-}$:$Nf1^{+/+}$ chimeras and human neurofibromas.

These lesions were further characterized by immunohistochemistry with an antibody recognizing S100, a protein expressed in mature Schwann cells and in most human neurofibromas and MPNSTs (*17*). As illustrated by the tumor shown in Fig. 1, E and G, S100-positive Schwann cells were observed exclusively associated with entrapped nerves (center) and were not found in the surrounding neoplastic tissue. In larger tumors in which the original nerve was disrupted (for example, Fig. 1, F and H), sparse S100 staining, associated with nerve remnants in the center of the lesion, were occasionally observed (Fig. 1H, right). In all cases (n = 25), only minimal S100 staining was observed in the lesion itself. The presence of S100-negative Schwann cells in the neurofibromas may be explained by their development within this model system, in which $Nf1^{-/-}$ cells are introduced at an early developmental stage (equivalent to E3.5). It is possible that the absence of S100 expression in these neurofibromas reflects a requirement for *Nf1* function in the differentiation of neural crest–derived precursors to S100-expressing Schwann cells in vivo. Indeed, neurofibromin is expressed early in Schwann cell differentiation in the mouse, 2 to 3 days before the onset of S100 expression (*18*). In contrast, in NF1 patients, neurofibromas arise from cells that are initially heterozygous for an *NF1* mutation. Cells within the human neurofibromas would be expected to become $NF1^{-/-}$, but in many cases this might occur after the onset of S100 expression, accounting for the high percentage of S100-positive neurofibromas in humans.

We next addressed the development of MPNSTs. Because these malignant tumors are often found emanating from primary plexiform benign lesions (*2, 15*), it is thought that additional (probably genetic) events are involved in the progression to malignancy. In fact, mutations in the *p53* tumor suppressor gene have been detected in human MPNSTs and therefore have been implicated in this progression step (*19*). As a means of creating a model for MPNST formation and establishing a causal role for *p53* mutations in the malignant lesions, mice with germ line mutations in *Nf1* and *p53* were generated on a mixed (129/sv × C57BL/6) genetic background. Because *Nf1* and *p53* are linked on chromosome 11 in mice (*20*), we initially generated animals carrying the *Nf1* and *p53* mutations on opposite chromosomes (NP trans) by crossing $Nf1^{+/-}$ and $p53^{+/-}$ mice. We also crossed these NP trans animals to wild-type animals to generate mice with both mutations on chromosome 11 (NP cis), which arise after meiotic recombination. Because complete chromosomal loss is the most common mutational mechanism by which second-hit mutations occur in mice (*21*), we expected most of these NP trans mice to undergo LOH at either the *Nf1* or the *p53* locus (but not both); we also thought this population of mice would exhibit a tumor phenotype reminiscent of the $Nf1^{+/-}$ and $p53^{+/-}$ parental animals (*10, 22*). In the NP cis mice, however, a chromosomal loss would be expected to result in LOH at both

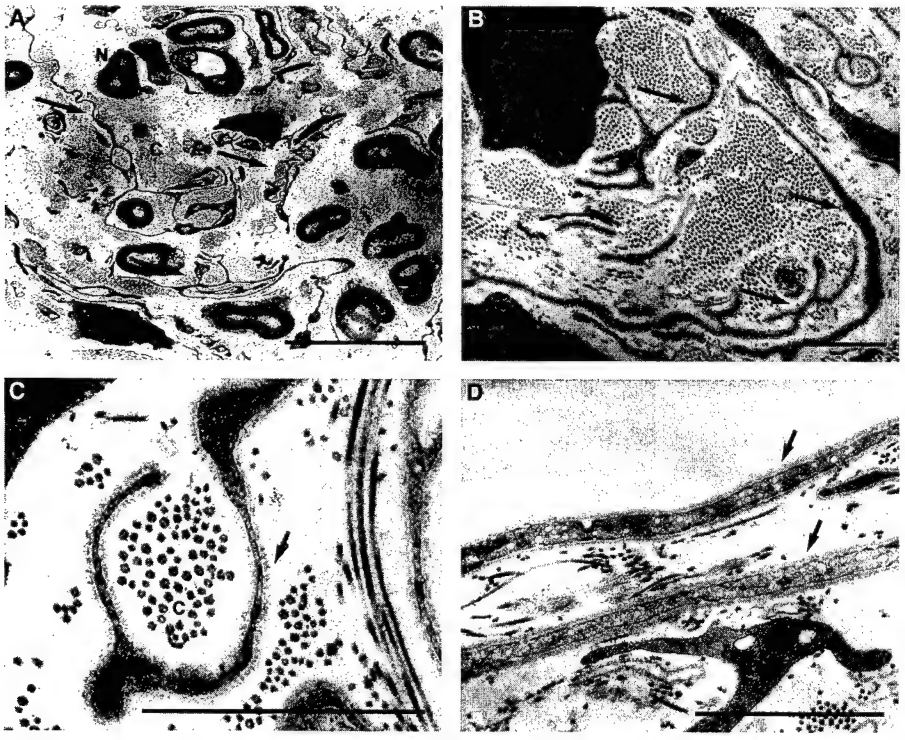

Fig. 2. Electron micrographs of murine neurofibromas. EM was performed on fixed tissue stained with lead citrate. (**A**) Low-power magnification of a neurofibroma containing myelinated axons (N), collagen bundles (C), and dissociated Schwann cells identified by arrows. Bar = 10 μm. Dissociated Schwann cells exhibit branching cytoplasmic processes (**B**) and surround collagen bundles (**C**). Note the continuous basal lamina (arrow) characteristic of Schwann cells. Bars = 1 μm. (**D**) Perineurial cells aligned in parallel arrays containing multiple pinocytotic vesicles and a basal lamina were also observed in murine neurofibromas. Cells exhibiting either discontinuous or continuous basal lamina (arrows) were observed in these tumors. Bar = 1 μm.

tumor suppressor loci simultaneously (a phenomenon we term co-LOH), resulting in cells deficient for both *Nf1* and *p53*.

As expected, NP trans animals succumbed to tumors more rapidly than mice heterozygous for a single mutation; they survived an average of 10 months and developed tumors similar to those found in mice with either single mutation (Fig. 3A). Southern blot analysis of tumor DNA ($n = 6$) revealed LOH of either the wild-type *Nf1* locus or the wild-type *p53* locus (*23*). In contrast, mice carrying *Nf1* and *p53* mutations in cis survived an average of only 5 months and exhibited a significant increase in the percentage of soft tissue sarcomas compared with mice of other genotypes ($Nf1^{+/-}$, 5%; *p53*, 57%; NP trans, 36%; NP cis, 81%). Furthermore, although NP trans animals exclusively develop osteo-, fibro-, rhabdomyo-, and hemangiosarcomas, about 30% of tumors from the NP cis animals stained positively for S100 and exhibited classic histological features of MPNSTs ($n = 28$) (Fig. 3B). The percentage of MPNSTs identified by these criteria is likely to be an underestimate because only 50% of human MPNSTs are S100-positive and due to the characteristic heterogeneity of this tumor type (*15, 24*). Importantly, loss of both wild-type alleles in tumors from the NP cis mice was consistently observed ($n = 12$) (*23*), which suggests that the loss of both genes cooperates in formation of these lesions in mice and supports a causal role for p53 mutations in development of MPNSTs in NF1 patients. The presence of S100-positive cells in the tumors from the NP cis mice contrasts with the analysis of neurofibromas in the model described above, where the lesions were universally $S100^-$. Although this pattern was unexpected, it supports the hypothesis that the timing of *Nf1* deficiency may be critical for expression of the S100 marker. Specifically, in contrast to the neurofibroma model, in the MPNSTs $Nf1^{-/-}$ cells arise from $Nf1^{+/-}$ cells, most likely at a later stage of gestation or in the adult mouse.

In summary, our data on the $Nf1^{-/-}$:$Nf1^{+/+}$ chimeras indicate that complete loss of *Nf1* is an obligate step in neurofibroma development and suggest that the prevalence of neurofibromin-deficient cells in the developing nerve is the rate-limiting factor in formation of this tumor in the mouse. It remains unclear why fewer of these cells arise in $Nf1^{+/-}$ mice than in human NF1 patients. Possible explanations include interspecies differences in lifespan, target cell number, or proliferative properties or interspecies differences in the mutability of the *NF1* locus. We have also demonstrated that mutations in *Nf1* and *p53* cooperate in the development of MPNSTs, which supports a causal role for p53 mutations in their formation. The development of these lesions might call into question the conclusion that a low rate of *Nf1* LOH limits the development of neurofibromas in $Nf1^{+/-}$ mice (see above). We hypothesize that the concomitant loss of *p53* and *Nf1* function that occurs in development of MPNSTs in the NP cis mice allows for the outgrowth of cells that otherwise would have undergone growth arrest or apoptosis were *Nf1* mutated alone. Previous work has shown that dysregulation of the Ras pathway in rat Schwann cells leads to growth arrest that can be overcome by inhibition of p53 function (*25*); oncogenic *ras* alleles can also induce p53-dependent growth arrest or apoptosis in human and mouse fibroblasts (*26*).

The simultaneous homozygosing of linked mutations by the process described here as co-LOH could have more general importance in tumor development, which could be strongly influenced either positively or negatively by the arrangement of linked germ line or somatically acquired mutations.

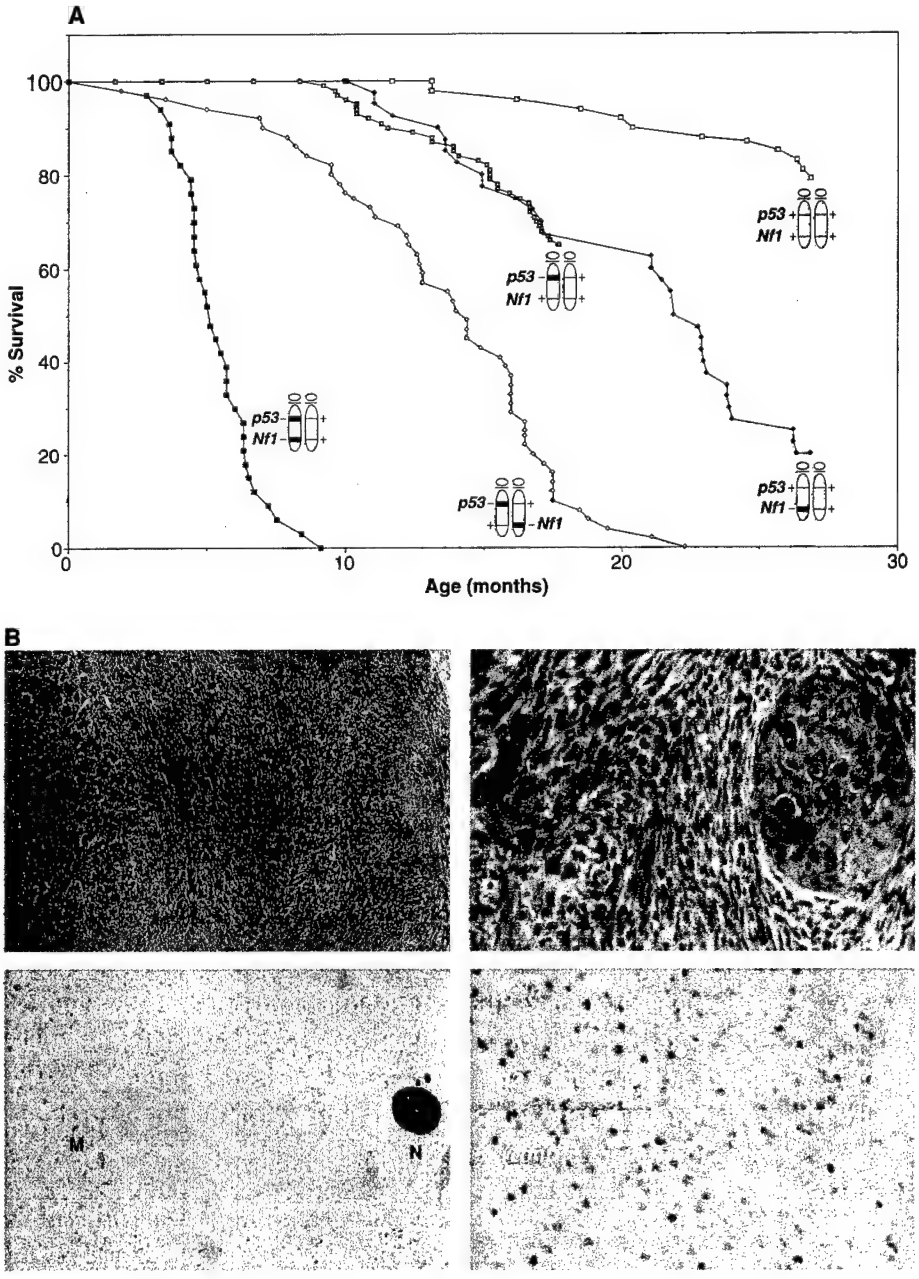

Fig. 3. Analysis of $Nf1^{+/-}$;$p53^{+/-}$ mice. (**A**) Survival curve of mice carrying *Nf1* and *p53* mutations on the same (NP cis) or opposing (NP trans) chromosomes. The $Nf1^{+/-}$ and $p53^{+/-}$ curves are identical to those published previously. We studied 51 NP trans animals, 34 NP cis animals, 19 wild-type animals, 37 $Nf1^{+/-}$ animals, and 41 $p53^{+/-}$ animals. (**B**) Sections of an MPNST arising in the rear flank of this animal were stained with H+E (upper) or S100 antibodies (lower). The nuclear S100 staining observed is also a characteristic of human MPNSTs and neurofibromas. MPNSTs were typically observed invading muscle (M) and were associated with nerves (N). Right panels are magnified views of left panels.

This effect may be more pronounced in mice than in humans, where LOH events are typically subchromosomal. Still, closely linked mutations that act synergistically or antagonistically could strongly affect the process of human tumor development through this mechanism.

Finally, we anticipate that both models will be critical in further characterization of tumorigenic mechanisms in NF1 and in the evaluation of potential therapies, such as compounds designed to inhibit Ras signaling, such as farnesyl transferase inhibitors (*27*).

References and Notes

1. D. A. Stumph, *Arch. Neurol.* **45**, 575 (1987).
2. V. M. Riccardi, *Neurofibromatosis: Phenotype, Natural History, and Pathogenesis* (Johns Hopkins Univ. Press, Baltimore, ed. 2, 1992).
3. J. L. Bader, *Ann. N.Y. Acad. Sci.* **486**, 57 (1986); D. G. Hope and J. J. Mulvihill, *Adv. Neurol.* **29**, 33 (1981).
4. R. M. Cawthon *et al.*, *Cell* **62**, 193 (1990); D. Viskochil *et al.*, *Cell* **62**, 187 (1990); M. R. Wallace *et al.*, *Science* **249**, 181 (1990).
5. G. A. Martin *et al.*, *Cell* **63**, 843 (1990); G. F. Xu *et al.*, *Cell* **63**, 835 (1990).
6. T. N. Basu *et al.*, *Nature* **356**, 713 (1992); G. Bollag *et al.*, *Nature Genet.* **12**, 144 (1996); E. DeClue *et al.*, *Cell* **69**, 265 (1992); A. Guha *et al.*, *Oncogene* **12**, 507 (1996).
7. K. M. Shannon *et al.*, *N. Engl. J. Med.* **330**, 597 (1994); E. Legius, D. A. Marchuk, F. S. Collins, T. W. Glover, *Nature Genet.* **3**, 122 (1993); W. Xu *et al.*, *Genes Chromosomes Cancer* **4**, 337 (1992).
8. S. D. Colman, C. A. Williams, M. R. Wallace, *Nature Genet.* **11**, 90 (1995); S. Sawada, *et al.*, *Nature Genet.* **14**, 110 (1996).
9. K. Daschner *et al.*, *Biochem. Biophys. Res. Commun.* **234**, 346 (1997); T. W. Glover *et al.*, *Genes Chromosomes Cancer* **3**, 62 (1991); R. A. Lothe *et al.*, *J. Neuropathol. Exp. Neurol.* **54**, 65 (1995); M. Stark, G. Assum, W. Krone, *Hum. Genet.* **96**, 619 (1995).
10. T. Jacks *et al.*, *Nature Genet.* **7**, 353 (1994).
11. C. I. Brannan *et al.*, *Genes Dev.* **8**, 1019 (1994).
12. *Nf1*$^{-/-}$ ES cells were generated with a two-step targeting strategy (*28*). D3-derived ES cell lines containing a disruption of one *Nf1* allele with a neomycin (*neo*) resistance gene replacing exon 31 have been described (*10*). These cells were retargeted with a second vector containing a hygromycin resistance gene in place of the *neo* gene, and two *Nf1*$^{-/-}$ lines (designated clones 6 and 47) were identified after selection in G418 and hygromycin. Mutations in both *Nf1* alleles were confirmed by Southern blot analysis as described in (*10, 21*).
13. Supplementary material is available at www.sciencemag.org/feature/data/1043163.shl.
14. Tissues were dissected, fixed in 10% formalin or Bouin's fixative and dehydrated in graded alcohol solutions. Paraffin-embedded tissues were cut in 4-μm sections and stained with hematoxylin and eosin (H+E).
15. J. M. Woodruff, in *Soft Tissue Tumors* (International Academy of Pathology, Baltimore, 1996).
16. *Nf1*$^{+/-}$ animals were crossed to mice carrying a β-gal transgene driven by the ubiquitously expressing *ROSA-26* promoter (*29*). *Nf1*$^{+/-}$, *ROSA-26*$^{+/-}$ ES cells were then generated de novo from delayed blastocysts (*30*), and the second *Nf1* allele was retargeted by using the hygromycin targeting construct used to generate the previous *Nf1*$^{-/-}$ cell lines (*12*).
17. Tissues were fixed in 10% formalin and processed as described. Immunohistochemical analysis using an S100 antibody (Dako) was done according to the manufacturer's instructions.
18. C. Kioussi and P. Gruss, *Trends Genet.* **12**, 84 (1996); D. H. Gutmann, J. L. Cole, F. S. Collins, *Prog. Brain Res.* **105**, 327 (1995).
19. A. G. Menon *et al.*, *Proc. Natl. Acad. Sci. U.S.A.* **87**, 5435 (1990); M. S. Greenblatt, W. P. Bennett, M. Hollstein, C. C. Harris, *Cancer Res.* **54**, 4855 (1994).
20. A. M. Buchberg, M. S. Buckwalter, S. A. Camper, *Mammalian Genome* **3**, S162 (1992).
21. C. Luongo, A. R. Moser, S. Gledhill, W. F. Dove, *Cancer Res.* **54**, 5947 (1994).
22. T. Jacks *et al.*, *Curr. Biol.* **4**, 1 (1994); L. A. Donehower *et al.*, *Nature* **356**, 215 (1992).
23. Supplementary material is available at www.sciencemag.org/feature/data/1043163.shl.
24. M. R. Wick, P. E. Swanson, B. W. Scheithauer, J. C. Manivel, *Am. J. Clin. Pathol.* **87**, 425 (1987).
25. A. J. Ridley, H. F. Paterson, M. Noble, H. Land, *EMBO J.* **7**, 1635 (1988).
26. A. W. Lin *et al.*, *Genes Dev.* **12**, 3008 (1998); M. Serrano, A. W. Lin, M. E. McCurrach, D. Beach, S. W. Lowe, *Cell* **88**, 593 (1997); M. S. Soengas *et al.*, *Science* **284**, 156 (1999).
27. J. B. Gibbs, A. Oliff, N. E. Kohl, *Cell* **77**, 175 (1994).
28. H. te Riele, E. R. Maandag, A. Clarke, M. Hooper, A. Berns, *Nature* **348**, 649 (1990).
29. G. Friedrich, P. Soriano, *Methods Enzymol.* **225**, 681 (1993).
30. E. J. Robertson in *Teratomas and Embryonic Stem Cells: A Practical Approach*, E. J. Robertson, Ed. (IRL Press, Oxford 1987), pp. 71–112.31.
31. A. I. McClatchey, I. Saotome, V. Ramesh, J. F. Gusella, T. Jacks, *Genes Dev.* **11**, 1253 (1997).

32. We thank D. Anthony, C. Fletcher, D. Housman, and M. Entman for helpful discussions and K. Mercer and D. Crowley for assistance with histology. K.C. was supported by an NNFF Young Investigator Award. This work was supported in part by a grant from the Department of the Army and the Medallion Foundation.

1 July 1999; accepted 14 October 1999

Nf1;Trp53 mutant mice develop glioblastoma with evidence of strain-specific effects

Karlyne M. Reilly[1], Dagan A. Loisel[1,4], Roderick T. Bronson[2], Margaret E. McLaughlin[1,3,4] & Tyler Jacks[1,4]

Astrocytomas are the leading cause of brain cancer in humans. Because these tumours are highly infiltrative, current treatments that rely on targeting the tumour mass are often ineffective. A mouse model for astrocytoma would be a powerful tool for dissecting tumour progression and testing therapeutics. Mouse models of astrocytoma have been designed to express oncogenic proteins in astrocytes, but have had limited success due to low tumour penetrance or limited tumour progression[1–3]. We present here a mouse model of astrocytomas involving mutation of two tumour-suppressor genes, *Nf1* and *Trp53*. Humans with mutations in *NF1* develop neurofibromatosis type I (NF1) and have increased risk of optic gliomas, astrocytomas and glioblastomas[4,5]. The *TP53* tumour suppressor is often mutated in a subset of astrocytomas that develop at a young age and progress slowly to glioblastoma (termed secondary glioblastomas, in contrast to primary glioblastomas that develop rapidly *de novo*[6–10]). This mouse model shows a range of astrocytoma stages, from low-grade astrocytoma to glioblastoma multiforme, and may accurately model human secondary glioblastoma involving *TP53* loss. This is the first reported mouse model of astrocytoma initiated by loss of tumour suppressors, rather than overexpression of transgenic oncogenes.

Although $Nf1^{+/-}$ mutant mice do not develop the benign lesions commonly seen in human NF1, such as neurofibromas and optic gliomas, *Nf1* and *Trp53* compound heterozygotes on a mixed C57BL/6×129S4/SvJae (B6,129) genetic background have been used to model malignant peripheral nerve sheath tumours[11,12] (MPNSTs). $Nf1^{+/-}$ mice show increased gliosis[13,14] and *TP53* is mutated in human astrocytoma[6–9]; thus, *Nf1* and *Trp53* compound heterozygotes were good candidates for developing a mouse model of astrocytoma. Because *Nf1* and *Trp53* are located within 7 cM of each other on mouse chromosome 11, we generated mice carrying mutations in *Nf1* and *Trp53* on the same chromosome (NPcis mice[11]). These mutations are rarely separated by recombination events and can be treated as a single mutation in genetic crosses. Because the tumour phenotype in *Nf1* heterozygotes has shown some strain-specific effects[15], we also crossed these NPcis mice on an enriched inbred background (C57BL/6 (B6)) to several inbred mouse strains to generate F1 progeny (C3H/HeJ×B6 (H×B6), CAST/EiJ×B6 (CA×B6), CBA/J×B6 (CB×B6) and SJL/J×B6 (S×B6)) for analysis.

We aged NPcis mice on the B6 and different F1 backgrounds until they developed various tumours (K.M.R. and T.J., unpublished data; see also Table 1, http://genetics.nature.com/supplementary_info/). Brain lesions were the most frequent tumour type seen on both the B6 and H×B6 backgrounds and the second most frequent tumour type seen on the CA×B6 and S×B6 backgrounds. These brain lesions range from the presence of diffuse cells with atypical nuclei to large, aggressive tumours bearing the hallmarks of glioblastoma multiforme. At the time of sacrifice, mice with more advanced tumours displayed ataxia and paralysis. After approximately 6 months of age, penetrance of the brain tumour phenotype approached 100% (92% on a B6 background), suggesting that if NPcis mice did not die of other shorter-latency tumours, they would all develop brain tumours.

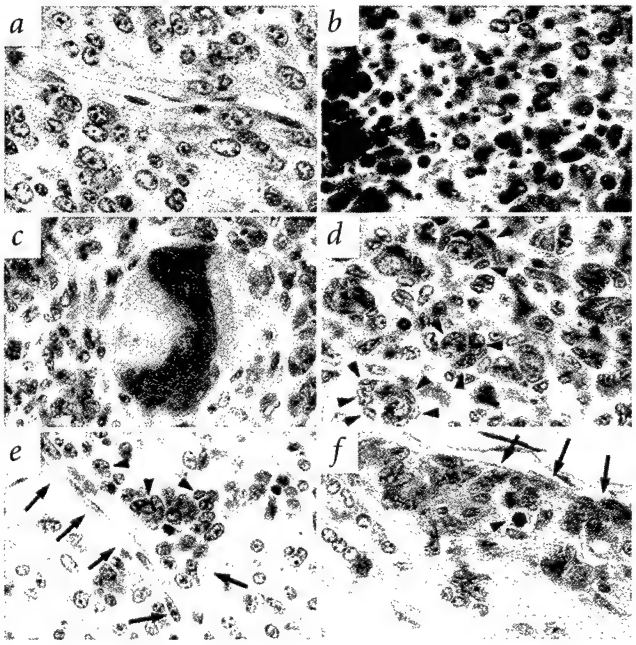

Fig. 1 Histology of astrocytomas in NPcis mice. The brain tumours in NPcis mice show histological hallmarks of human astrocytomas and glioblastomas. Sections are stained with haematoxylin and eosin. Glioblastoma multiforme in humans is characterized by the presence of either vascular proliferation or necrosis. Advanced tumours in NPcis mice show evidence of new blood vessel formation (although multilayering of endothelial cells is not detected) (***a***) and of necrosis (***b***). We observed multinucleated giant cells (**c**) in 22–36% of all brain lesions depending on the genetic background (27% overall), characteristic of glioblastoma in humans. Because astrocytic tumour cells are very migratory, leading to highly infiltrative tumours, they tend to cluster around structures in the brain, forming 'secondary structures'. Among the types of secondary structures formed are perineurial structures around neurons, also known as 'satellitosis' (neurons indicated by an asterisk and tumour cells indicated by arrowheads) (***d***), perivascular structures around blood vessels (vessel indicated by arrows and tumour cells indicated by arrowheads) (**e**), and accumulation of cells in the subpial zone of the cortex (pial surface marked by arrows, arrowhead indicates mitosis amid the tumour cells) (***f***). Although we generally did not find tumours in the cerebellum, they occurred in the olfactory bulb, throughout the cortex (including the corpus callosum), in the brainstem and down into the spine, similar to human astrocytomas. They often exited the olfactory bulb or cortex into the nasal cavity or leptomeninges (see also Fig. 3*g*). *c,d*, Taken from the same tumour specimen.

[1]*Department of Biology and Center for Cancer Research, Massachusetts Institute of Technology, Cambridge, Massachusetts, USA.* [2]*Department of Pathology, Tufts University Schools of Medicine and Veterinary Medicine, Boston, Massachusetts, USA.* [3]*Department of Pathology, Brigham and Women's Hospital, Boston, Massachusetts, USA.* [4]*Howard Hughes Medical Institute, Massachusetts Institute of Technology, Cambridge, Massachusetts, USA. Correspondence should be addressed to T.J. (e-mail: tjacks@mit.edu).*

Fig. 2 Glioblastoma multiforme in an NPcis mouse on a (H×B6)F1 background. This figure shows a tumour in the thalamus of an NPcis mouse with the criteria of a human glioblastoma multiforme. ***a***, A low-power magnification of the haematoxylin and eosin stained sagittal section. Anterior is to the left and dorsal is up. The pituitary (P) and cerebellum (C) are shown for reference. The tumour shows accumulation of cells dorsally and diffuse, infiltrative growth (IG) ventrally and posteriorly. In addition to atypical nuclei and mitotic figures (arrows) (***b***,***c***), this tumour also shows microscopic foci of necrosis (shown in Fig. 1*b*). The tumour stains very strongly for GFAP (*b*), but not for synaptophysin (c), indicating it is glial, not neural, in origin.

In humans, astrocytomas are graded according to defined histological criteria, as determined by the World Health Organization[16,17] (WHO). We did not see any well-circumscribed benign lesions similar to pilocytic astrocytomas (WHO I) in NPcis mice. All NPcis mice lesions contained elongated astrocytic nuclei with irregular contours, similar to low-grade diffuse astrocytomas (WHO II). Similar to human anaplastic astrocytomas (WHO III) that are defined by increased mitotic activity, NPcis mouse brains often exhibited mitotic figures, with a subset exhibiting focal tumour masses. Although rare, we observed necrosis in four tumours (from a total of 100 animals analysed; Fig. 1*b*), indicating that these tumours can progress to glioblastoma multiforme (WHO IV; Fig. 2), as well as atypical or excessive blood vessels in four tumours (Fig. 1*a*). NPcis tumours also contained multinucleated giant cells (Fig. 1*c* and Fig. 3*d*) and formed 'secondary structures' within the brain[18] (Fig. 1*d–f*), characteristic of glioblastoma[16].

To confirm that these brain tumours were glial in origin (as opposed to neural), we stained 40 focal tumours with both astrocytic and neural markers (see Table 1, http://genetics.nature.com/supplementary_info/). Glial fibrillary acidic protein (GFAP) is a marker of glial cells and astrocytoma in humans[19]. Of the 40 tumours tested, 28 showed positive GFAP staining of tumour cells (Fig. 2*b* and Fig. 3*b*,*h*). The remaining 12 showed astrocyte staining within the tumour that could not be distinguished from a reactive astrocyte pattern (Fig. 3*e*). These tumours may contain GFAP-positive tumour cells, but the morphology of the positive cells did not allow us to identify them conclusively as tumour cells. The possible lack of GFAP staining in these tumours may result from dedifferentiation of tumour cells as the tumour progresses, consistent with the finding in humans that more anaplastic astrocytomas do not show GFAP immunoreactivity[19], or may indicate that the tumour arose from a neural stem cell before differentiation (although these tumours were negative for the marker nestin; see Table 1, http://genetics.nature.com/supplementary_info/). Of the 40 tumours stained for GFAP, we stained 34 with anti-synaptophysin antibodies (a marker of neural cells and neuroectodermal tumours[20]) and found no staining of tumour cells (Fig. 2*c* and Fig. 3*c*,*f*).

We analysed tumour tissue for loss of the wild-type alleles of *Nf1* and *Trp53*. To obtain pure tumour DNA samples from these highly infiltrative tumours, we used laser capture microdissection[21] on focal tumours. Of the five tumours analysed, three showed loss of wild-type *Nf1* and *Trp53* (Fig. 4). The remaining two tumours may carry point mutations or small deletions that are not detected by PCR, or the presence of the wild-type allele may be due to contaminating normal cells trapped within the tumour sample.

We cultured tumour cells from NPcis mice showing paralysis or ataxia. Cloned cell lines show stellate morphology and loss of wild-type *Nf1* and *Trp53* (Fig. 5). All cell lines formed tumours when injected subcutaneously into the flanks of nude mice. These tumours showed a more spindle-cell morphology than the original tumours, but stained with the S100 marker, consistent with glial origin (Fig. 5).

A study on variable expressivity within families with NF1 has demonstrated the importance of modifier genes in the benign aspects of the disease[22]. To test whether modifier genes similarly affect malignancies associated with NF1, we analysed (H×B6),

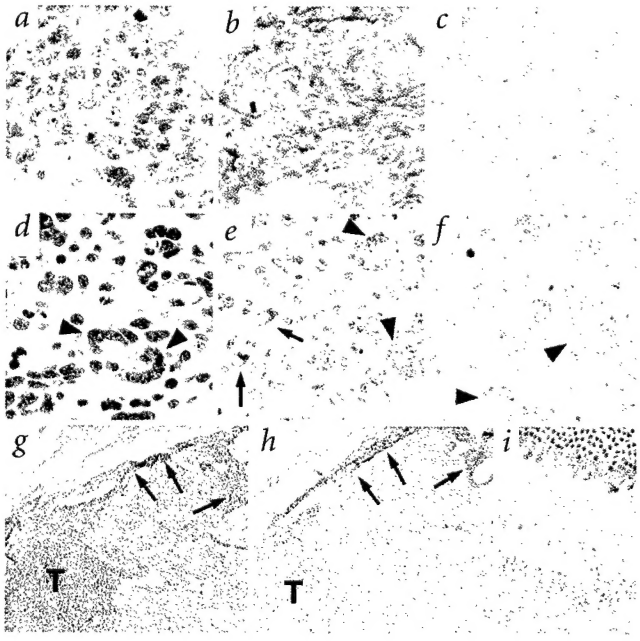

Fig. 3 Immunohistochemistry of astrocytomas in NPcis mice. Tumours were stained with an astrocytic marker, GFAP (***b***,***e***,***h***), or a neural marker, synaptophysin (***c***,***f***,***i***) (antibody stain shown in brown and nuclei counterstained blue). Normal astrocytes or neurons on the brain sections are internal controls for immunohistochemistry. Haematoxylin and eosin stained sections are shown for comparison (***a***,***d***,***g***). *a–c*, A tumour in the olfactory bulb that has exited into the nasal cavity and stains strongly for GFAP (*b*), but not synaptophysin (*c*). *d–f*, A tumour with many multinucleated giant cells (arrowheads) in the frontal lobe of the cortex that shows staining of astrocytes by GFAP (arrows) within the tumour (e), but not widespread staining. These astrocytes (indicated by arrows in e) appear abnormal and possibly tumorigenic, but we cannot rule out the possibility that they may be reactive astrocytes trapped within the tumour. These tumour cells did not stain with synaptophysin (*f*), although neuronal processes extending through the region of the tumour show faint synaptophysin staining. *g*,*h*, A low-power magnification of a tumour (T) in the frontal lobe (anterior to the left, ventral is up) that has exited the cortex into the leptomeninges (arrows). GFAP staining was highly variable in the tumour tissue and was much stronger in the leptomeningeal part of the tumour (arrows) than in the cortical part (T) (*h*). None of the tumours tested showed positive staining for synaptophysin, although in four tumours of the olfactory bulb or pons, neurons trapped within the tumour stained for synaptophysin. *i*, An example of synaptophysin staining in the retina, as an internal control.

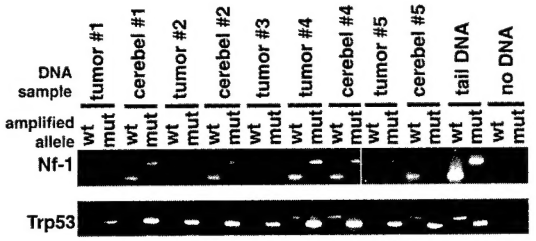

Fig. 4 Astrocytomas show loss of the wild-type alleles of *Nf1* and *Trp53*. We microdissected tumour tissue and amplified the wild-type and mutant alleles of *Nf1* and *Trp53* by PCR. Because we generally did not see these tumours forming in the cerebellum, and because the cerebellum is densely nuclear and therefore a good source of DNA, we microdissected the granule cell layer of the cerebellum as a control for the presence of the wild-type allele. The figure shows loss of the wild-type chromosome in the region of *Nf1* and *Trp53* in three of five samples. Tumour 1 is a multifocal tumour with mitotic figures and multinucleated giant cells that stained strongly for GFAP. Tumour 2 is a diffuse tumour mass in the brainstem that showed sparse staining for GFAP. Tumour 3 is a highly infiltrative tumour with mitotic figures and leptomeningeal spread that showed sparse staining for GFAP. Tumour 4 is a dense tumour with mitotic figures and giant cells that stained strongly for GFAP. Tumour 5 is a dense, highly pleomorphic tumour with mitotic figures, giant cells and satellitosis around trapped neurons. It stained strongly for GFAP.

(CA×B6), (CB×B6) and (S×B6) F1 progeny for changes in tumour phenotype relative to the B6 parental strain (Fig. 6). The cross to the SJL/J strain caused a significant reduction in focal brain tumours (χ^2, P=0.0035), and the cross to the CAST/EiJ strain showed a reduction in focal brain tumours that was suggestive, but not statistically significant (χ^2, P=0.17). NPcis (S×B6)F1 progeny did not live longer in the absence of brain tumours (Fig. 6*b*), but instead died of other, early forming tumours, precluding the development of brain tumours. NPcis (S×B6)F1 progeny showed an increase in soft-tissue sarcomas that is suggestive, but not statistically significant (χ^2, P=0.18; K.M.R. and T.J., unpublished data). These soft-tissue sarcomas tended to occur at younger ages than brain lesions in NPcis mice and may account for the reduction in brain tumours in the (S×B6)F1 background.

We classified the brain tumours into four grades on the basis of histological criteria. This classification is related to, but not identical to, the WHO classification (Fig. 6*a*, see legend). Mice dying at older ages tended to have higher-grade lesions, suggesting that this model may be useful for studying progression of astrocytomas. Although we did not see any grade 4 lesions in NPcis mice on the parental B6 background, we did observe grade 4 tumours in all three strains of F1 progeny (Fig. 6*a*), suggesting an effect of genetic background on the extent of tumour progression. The effect of background on the development of these tumours and their progression may allow us to optimize this model system using different mouse strains.

We have presented here a mouse model for secondary glioblastoma involving loss of *TP53* in humans. In addition to modelling spontaneous glioblastomas, these NPcis mice extend our previous model of the malignancies associated with human NF1 (refs 11,12). Although $Nf1^{+/-}$ mice do not develop the benign lesions of peripheral nervous system glia (neurofibromas) or central nervous system glia (optic gliomas) seen in NF1 patients[23], the combination of *Nf1* and *Trp53* mutations leads to malignant tumours of glia in both the peripheral and central nervous system (MPNSTs (ref. 24) and astrocytomas, respectively). We hypothesize that dysregulation of Ras signalling through loss of the rasGAP function of Nf1 gives Schwann cells and astrocytes a growth advantage, as evidenced by the formation of neurofibromas in *Nf1*-null chimaeras and increased gliosis in *Nf1* heterozygotes. The *Nf1* mutation may mimic the mitogenic stimulus provided by amplification and/or mutation of *EGFR* and *PDGFR* in human astrocytomas. As in human astrocytomas, the loss of *Trp53* function may facilitate the progression to malignancy in this model. We have further extended the NF1 model by demonstrating the role of modifier genes in different strains of mice. Previous characterizations of NPcis mice on a (B6,129) mixed background[11,12] did not identify brain tumours as a significant cause of death in these mice, and we are currently investigating whether the 129 strain carries resistance genes for these tumours. Comparison of NPcis mice on a B6 background with (S×B6)F1 or (CA×B6)F1 mice revealed the role of modifier genes in both tumour initiation and progression. We are currently investigating backcross progeny to identify modifier genes by quantitative trait mapping approaches. We believe these NPcis mice are a good model for secondary glioblastomas that in humans progress from lower grades of astrocytoma and involve loss of *TP53*.

Methods

Construction of *Nf1;Trp53 cis* mice. We bred $Nf1^{+/-}$ mice on a mixed C57BL/6, 129S4/SvJae background to wild-type C57BL/6 (B6) mice for five generations and then crossed to $Trp53^{+/-}$ mice inbred on B6 (Jackson Laboratory). We bred the resulting double heterozygotes in '*trans*' to wild-type B6 mice and progeny were scored by PCR genotyping[23,25] for the presence

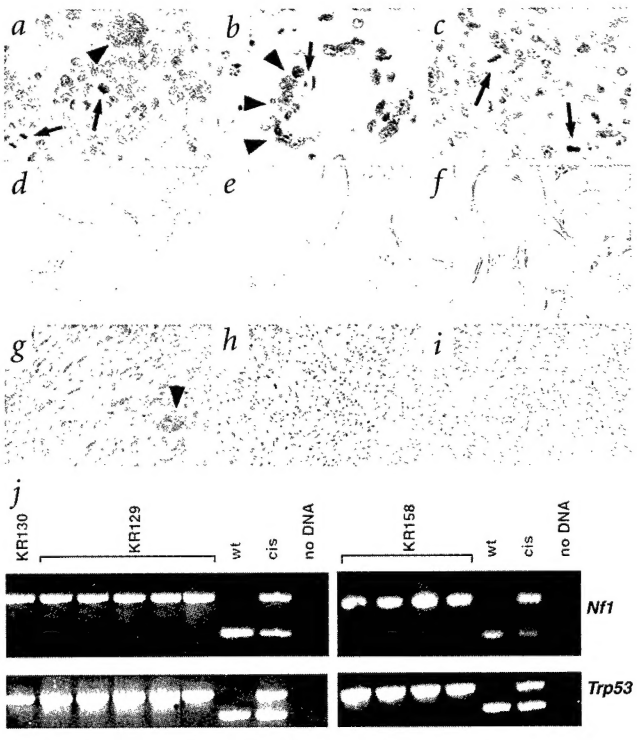

Fig. 5 Tissue culture of astrocytomas. We killed mice displaying obvious signs of brain tumours (ataxia, paralysis and so on) and put a parasagittal half of the brain into culture, with the other half of the brain fixed for histology (n=5). This figure shows the histology and cell morphology of three of the tumours and their corresponding cloned cell lines, as well as immunohistochemistry for S100 on sections of tumours grown subcutaneously from injected cell lines in nude mice. All cell lines showed a stellate morphology. *a,d,g*, A tumour from a (S×B6)F1 background with giant cells (arrowheads) and mitotic figures (arrows) (***a***), the corresponding cell line (***d***) and the xenograft stained with S100 (***g***). *b,e,h*, A tumour from a (CB×B6)F1 background with accumulation of tumour cells into secondary structures around blood vessels (arrowheads) and a mitotic figure (arrow) (***b***), the corresponding cell line (***e***) and S100 staining of the xenograft (***h***). *c,f,i*, A tumour from a B6 background with a high mitotic index (arrows) (***c***), the corresponding cell line (***f***) and the S100 staining of the xenograft (***i***). Multiple single-cell clones of each cell line showed loss of the wild-type alleles of *Nf1* and *Trp53* (***j***). KR130 corresponds to the tumour shown in (*a,d*), KR129 corresponds to the tumour shown in (*b,e*), and KR158 corresponds to the tumour shown in (*c,f*).

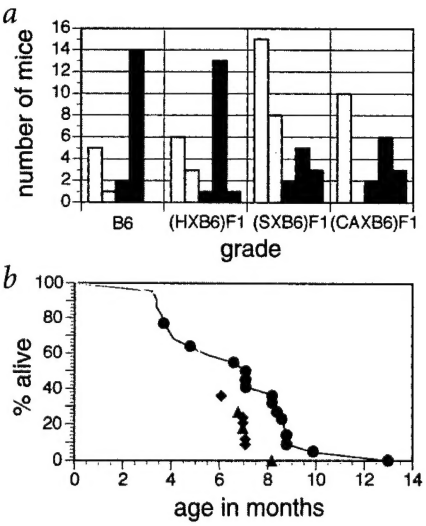

Fig. 6 Incidence of brain tumours in NPcis mice. ***a***, We graded tumours according to histological criteria. Grade 0 (cyan) indicates no brain lesion was identified in the sections analysed; grade 1 (green) lesions have diffuse cells with atypical nuclear morphology; grade 2 (magenta) lesions have diffuse atypical cells and mitotic figures; grade 3 (blue) lesions are focal tumours with varying degrees of cellularity; and grade 4 (red) tumours show evidence of excessive or aberrant blood vessels and/or necrosis. The histogram shows the distribution of tumour grade for NPcis mice of four different genetic backgrounds, the parental B6 strain and three F1 strains (H×B6, S×B6 and CA×B6). In the B6 background, 77% of mice developed a brain lesion (n=2). In the (H×B6)F1 background, 75% of mice developed a brain lesion (n=24). In the (S×B6)F1 background, 55% of mice developed a brain lesion (n=33). In the (CA×B6)F1 background, 58% of mice developed a brain lesion (n=21). The distribution shows that the C3H strain does not modify the grade distribution of the B6 strain, whereas SJL and CAST backgrounds reduce the proportion of focal tumours (grades 3 and 4) in the population. The reduction of focal tumours in (S×B6)F1 is statistically significant (χ^2, P=0.0035), whereas the reduction in (CA×B6)F1 may be suggestive of an effect, but is not significant (χ^2, P=0.17). Both the SJL and CAST backgrounds may also cause a change in tumour progression as evidenced by changes in the proportion of the different tumour grades. ***b***, Grade 3 (blue) and 4 (red) tumours in the (S×B6)F1 and B6 strains are graphed on top of the survival curve for each strain ((S×B6)F1 in green and B6 in blue), showing that the two strains develop focal tumours at similar ages. This suggests that the reduction in the number of brain tumours observed in the (S×B6)F1 mice is not due to resistance to developing brain tumours, but rather to an increased susceptibility to early forming tumour types. The mice that do not develop brain tumours are dying earlier of other tumours (K.M.R. and T.J., unpublished data). We have not yet identified a background showing reduced tumours in the later part of the survival curve, suggesting true resistance to the development of brain lesions. The difference in the survival of B6 mice and (S×B6)F1 mice in the later part of the curve is significant (log-rank test, P=0.0043), and may be linked to the lack of grade 4 tumours in B6 mice. This suggests that tumours in B6 mice may progress more slowly than those in other strains.

of both mutations, indicating the germline recombination had placed the two mutations on the same chromosome in '*cis*'[11,12]. The resulting founder *Nf1;Trp53 cis* mice (NPcis) are inbred the equivalent of seven generations, and mice used here were from further backcrosses of these mice to B6 (backcross generations 8 to 11). We crossed NPcis mice on B6 to four strains (C3H/HeJ, CAST/EiJ, CBA/J and SJL/J; Jackson Laboratory) to generate F1 progeny for analysis.

Histological analysis of tumours. We aged NPcis sibling sets over a period of 13 months until all mice developed tumours. We observed the NPcis mice several times weekly for signs of tumours or morbidity and killed them by CO_2 asphyxiation. We killed mice that were sick due to tumour burden and examined all major organs both grossly and histologically. We fixed soft tissues in 10% neutral buffered formalin and heads along with other bony tissues in Bouin's fixative. We embedded tissue in paraffin, sectioned, and stained with haematoxylin and eosin. Brains were scored for the presence of atypical nuclei, mitotic figures, tumour masses, multinucleated giant cells, excessive or atypical blood vessels and necrosis independently by K.M.R. and a veterinary pathologist (R.T.B.), and compared with human brain lesions by a neuropathologist (M.E.M.). These histological characteristics were never seen in wild-type B6 mouse brains (n=8). In determining whether the brain tumours were primary tumours or metastases from other tumours, we analysed the entire animal and compared cell morphology between the different tumour types. Only primary brain tumours are being included in this analysis.

Laser capture microdissection and analysis of wild-type copies of *Nf1* and *Trp53*. To examine loss of wild-type copies of *Nf1* and *Trp53*, we removed half of the brain from the skull and fixed in 10% neutral buffered formalin for 16 to 24 h, whereas the remainder of the skull was fixed in Bouin's for one week. We stained sections of formalin-fixed tissue with haematoxylin/eosin and isolated tumour tissue by laser capture microdissection[21]. We digested dissected material overnight with proteinaseK, heat inactivated it and used it directly in PCR reactions. We amplified the wild-type allele of *Nf1* with the primers Nf1com (5′–TGTCGTTTGGCATCATCATT–3′) and Nf1x31 (5′–GCAAATCTAGTATTGAATTGAAGCA–3′), and the mutant allele of *Nf1* with the primers Nf1com and Nf1neo3′ (5′–CTTGCAAAACCACACT GCTC–3′). We amplified the wild-type allele of *Trp53* with the primers X7 (5′–TATACTCAGAGCCGGCC–3′) and I6.2073 (5′–TGCCGAACAGGTG-GAATATC–3′), and the mutant allele of *Trp53* with the primers: X7 and Trp53neo3′ (5′–GCCTGAAGAACGAGATCAGC–3′). We ran PCR reactions on a 3% Metaphor agarose (FMC), 1×TBE gel at 5 V/cm and visualized the products by ethidium bromide staining. Because the tumours analysed originally were not suitable for PCR after microdissection due to fixation in Bouin's, the microdissected tumours represent additional tumours not included in the survival analysis and initial characterization (see Table 1, http://genetics.nature.com/supplementary_info/).

Immunohistochemistry of brain tumours. We stained Bouin's-fixed, paraffin-embedded samples for GFAP (Dako), synaptophysin (Dako) and nestin (Developmental Hybridoma Studies Bank). We stained formalin-fixed, paraffin-embedded nude mouse xenografts with S100 (Dako). We blocked endogenous peroxidases using 0.3% hydrogen peroxide in methanol. We pretreated samples stained for synaptophysin and nestin in citrate buffer for 2 h at 80 °C to unmask antigens. We detected all antibodies by biotin-conjugated secondary antibodies (Dako) and ABC (Vector), using DAB (Vector) as a substrate for peroxidase, and counterstained with haematoxylin.

Generation of tumour cell lines. We killed mice with clear behavioural manifestations suggesting the presence of a brain tumour and cultured half of their brain. We fixed the remaining half of the brain in the skull in Bouin's for pathology. We subdivided brain tissue into four pieces along the dorsal-ventral axis and minced it in trypsin. After digestion in trypsin and DNaseI for 30 min, we passed the cells through a 70-μm filter and plated on 10-cm tissue culture plates in DME/10% IFS/glutamine/penicillin/streptomycin. We grew cells to 5 confluent 10-cm plates and single-cell cloned by limiting dilution in 96-well plates. We froze down the cells when single-cell clones reached 5 confluent 10-cm plates (n=5 brains, 4–8 clones per brain). At this stage we collected DNA and assayed for the wild-type copies of *Nf1* and *Trp53* by PCR (refs 23,25).

Injection of cell lines into nude mice. We injected 1×10^6 cells subcutaneously into the flanks of nude mice (The Jackson Laboratory) in duplicate. We used E1A- and H-ras-transformed *Trp53*-null mouse embryonic fibroblasts[26] (MEFs) as a positive control for tumour growth, and Rb null;p21 null MEFs (ref. 27) as a negative control. We analysed tumours at 6–7 weeks when tumours were at least 1 cm in diameter.

Statistical analysis of NPcis tumours on different strain backgrounds. We compared tumour latency and survival curves between the F1 strain and the parental strain by Kaplan-Meier survival analysis using the log-rank test in STATA. We analysed differences in the numbers of tumours seen in the F1 strain compared with the parental strain by a χ^2 test in Microsoft Excel 98.

Acknowledgements

We thank D. Crowley, N.H. Fong, K. Mercer and B. Williams for technical assistance; A. Charest, J. Sage, K. Cichowski, K. Olive, K. Johnson, K. Tsai and D. Tuveson for discussions; C. Whittaker, C. Fry, M. Bryce and J. Reilly for assistance in preparation of the manuscript and figures; and S. Shih for assistance with inbreeding of Nf1$^{+/-}$ mice. K.M.R. is supported by a post-doctoral fellowship from the Leukemia & Lymphoma Society. T.J. is an Associate Investigator of the Howard Hughes Medical Institute. This work was supported in part by a grant from the Department of the Army and the Medallion Foundation.

Received 23 January; accepted 5 June 2000.

1. Danks, R. *et al.* Transformation of astrocytes in transgenic mice expressing SV40 T antigen under the transcriptional control of the glial fibrillary acidic protein promoter. *Cancer Res.* **55**, 4302–4310 (1995).
2. Holland, E., Hively, W., DePinho, R. & Varmus, H. A constitutively active epidermal growth factor receptor cooperates with disruption of G1 cell-cycle arrest pathways to induce glioma-like lesions in mice. *Genes Dev.* **12**, 3675–3685 (1998).
3. Weissenberger, J. *et al.* Development and malignant progression of astrocytomas in GFAP-v-*src* transgenic mice. *Oncogene* **14**, 2005–2013 (1997).
4. Huson, S. & Hughes, R. *The Neurofibromatoses: A Pathogenetic and Clinical Overview* (Chapman & Hall Medical, London, 1994).
5. Sorensen, S.A., Mulvihill, J.J. & Nielsen, A. Long-term follow-up of von Recklinghausen neurofibromatosis. Survival and malignant neoplasms. *N. Engl. J. Med.* **314**, 1010–1015 (1986).
6. Watanabe, K. *et al.* Incidence and timing of *p53* mutations during astrocytoma progression in patients with multiple biopsies. *Clin. Cancer Res.* **3**, 523–530 (1997).
7. Watanabe, K. *et al.* Overexpression of the EGF receptor and *p53* mutations are mutually exclusive in the evolution of primary and secondary glioblastomas. *Brain Pathol.* **6**, 217–223 (1996).
8. van Meyel, D.J. *et al. p53* mutation, expression, and DNA ploidy in evolving gliomas: evidence for two pathways of progression. *J. Natl Cancer Inst.* **86**, 1011–1017 (1994).
9. Rasheed, B.K. *et al.* Alterations of the *TP53* gene in human gliomas. *Cancer Res.* **54**, 1324–1330 (1994).
10. Lang, F.F., Miller, D.C., Koslow, M. & Newcomb, E.W. Pathways leading to glioblastoma multiforme: a molecular analysis of genetic alterations in 65 astrocytic tumors. *J. Neurosurg.* **81**, 427–436 (1994).
11. Cichowski, K. *et al.* Mouse models of tumor development in neurofibromatosis type I. *Science* **286**, 2172–2176 (1999).
12. Vogel, K. *et al.* Mouse tumor model for neurofibromatosis type 1. *Science* **286**, 2176–2179 (1999).
13. Rizvi, T. *et al.* Region-specific astrogliosis in brains of mice heterozygous for mutations in the neurofibromatosis type 1 (*Nf1*) tumor suppressor. *Brain Res.* **816**, 111–123 (1999).
14. Gutmann, D. *et al.* Haploinsufficiency for the neurofibromatosis 1 (NF1) tumor suppressor results in increased astrocyte proliferation. *Oncogene* **18**, 4450–4459 (1999).
15. Tischler, A., Shih, T., Williams, B. & Jacks, T. Characterization of pheochromocytomas in a mouse strain with a targeted disruptive mutation of the neurofibromatosis gene *Nf1*. *Endocrine Pathol.* **6**, 323–335 (1995).
16. Kleihues, P. & Cavenee, W. *Pathology and Genetics of Tumours of the Nervous System* (International Agency for Research on Cancer, Lyon, 1997).
17. Kleihues, P., Burger, P.C. & Scheithauer, B.W. The new WHO classification of brain tumours. *Brain Pathol.* **3**, 255–268 (1993).
18. Scherer, H. The forms of growth in gliomas and their practical significance. *Brain* **63**, 1–35 (1940).
19. Marsden, H.B., Kumar, S., Kahn, J. & Anderton, B.J. A study of glial fibrillary acidic protein (GFAP) in childhood brain tumours. *Int. J. Cancer* **31**, 439–445 (1983).
20. Gould, V.E. *et al.* Synaptophysin: a novel marker for neurons, certain neuroendocrine cells, and their neoplasms. *Hum. Pathol.* **17**, 979–983 (1986).
21. Bonner, R. *et al.* Laser capture microdissection: molecular analysis of tissue. *Science* **278**, 1481–1483 (1997).
22. Easton, D., Ponder, M., Huson, S. & Ponder, B. An analysis of variation in expression of neurofibromatosis (NF) type 1 (NF1): evidence for modifying genes. *Am. J. Hum. Genet.* **53**, 305–313 (1993).
23. Jacks, T. Tumor predisposition in mice heterozygous for a targeted mutation in *Nf1*. *Nature Genet.* **7**, 353–361 (1994).
24. Menon, A. *et al.* Chromosome 17p deletions and p53 gene mutations associated with the formation of malignant neurofibrosarcomas in von Recklinghausen neurofibromatosis. *Proc. Natl Acad. Sci. USA* **87**, 5435–5439 (1990).
25. Jacks, T. Tumor spectrum analysis in *p53*-mutant mice. *Curr. Biol.* **4**, 1–7 (1994).
26. Lowe, S., Jacks, T., Housman, D. & Ruley, H. Abrogation of oncogene-associated apoptosis allows transformation of *p53*-deficient cells. *Proc. Natl Acad. Sci. USA* **91**, 2026–2030 (1994).
27. Brugarolas, J., Bronson, R. & Jacks, T. p21 is a critical CDK2 regulator essential for proliferation control in *Rb*-deficient cells. *J. Cell Biol.* **141**, 503–514 (1998).